J. Fluid Mech. (1998), *vol.* 367, *pp.* 255–289. Printed in the United Kingdom

Self-similarity of time-evolving plane wakes

By ROBERT D. MOSER[1], MICHAEL M. ROGERS[2] AND DANIEL W. EWING[3]†

[1]Department of Theoretical and Applied Mechanics, University of Illinois, Urbana, IL 61801, USA

[2]NASA-Ames Research Center, Moffett Field, CA 94035, USA

[3]Department of Mechanical and Aerospace Engineering, State University of New York at Buffalo, Amherst, NY 14260, USA

(Received 29 July 1996 and in revised form 16 January 1998)

Direct numerical simulations of three time-developing turbulent plane wakes have been performed. Initial conditions for the simulations were obtained using two realizations of a direct simulation from a turbulent boundary layer at momentum-thickness Reynolds number 670. In addition, extra two-dimensional disturbances were added in two of the cases to mimic two-dimensional forcing. The wakes are allowed to evolve long enough to attain approximate self-similarity, although in the strongly forced case this self-similarity is of short duration. For all three flows, the mass-flux Reynolds number (equivalent to the momentum-thickness Reynolds number in spatially developing wakes) is 2000, which is high enough for a short $k^{-5/3}$ range to be evident in the streamwise one-dimensional velocity spectra.

The spreading rate, turbulence Reynolds number, and turbulence intensities all increase with forcing (by nearly an order of magnitude for the strongly forced case), with experimental data falling between the unforced and weakly forced cases. The simulation results are used in conjunction with a self-similar analysis of the Reynolds stress equations to develop scalings that approximately collapse the profiles from different wakes. Factors containing the wake spreading rate are required to bring profiles from different wakes into agreement. Part of the difference between the various cases is due to the increased level of spanwise-coherent (roughly two-dimensional) energy in the forced cases. Forcing also has a significant impact on flow structure, with the forced flows exhibiting more organized large-scale structures similar to those observed in transitional wakes.

1. Introduction

The plane wake studied here is one of several canonical free-shear flows that are used as test flows for the development of turbulence models and turbulence control strategies. These flows are also of interest in many practical engineering applications such as high-lift airfoil configurations where one lifting surface (a flap) may operate in or near the wake of an upstream component. The numerical simulations reported here are the first of several to be performed to provide data for turbulence modelling relevant to such a configuration.

The evolution of the wake is generally broken up into three regions: the near field, an intermediate field, and the far or 'equilibrium' region of the wake. It is

† Current address: Department of Mechnical Engineering, McMaster University, Hamilton, Ontario, L8S 4L7, Canada.

widely recognized that the dynamics of the large-scale coherent structures in the flow play a dominant role in the first two regions of the flow; however, their role in the latter region is not as well understood. It is also known that in this latter region the governing equations for the single-point moments admit similarity solutions in the small-deficit (or infinite downstream distance, x) limit, where the thickness of the layer grows as $x^{1/2}$. Traditionally, it was argued (e.g. Townsend 1976) that the effects of differences in the initial conditions die out in the far field, so that the asymptotic state of all wakes is universal. This hypothesis was not supported by later experimental evidence. For example, Wygnanski, Champagne & Marasli (1986) reported non-dimensional wake growth rates between 0.29 and 0.41 depending on the body used to generate the wake. Even larger growth rates could be achieved if two-dimensional forcing was used to excite the large-scale motions (Wygnanski *et al.* 1986; Marasli, Champagne & Wygnanski 1992). The profiles of the scaled turbulent normal stresses in the wake far field were also different, as predicted in a similarity analysis by George (1989), despite the collapse of the mean velocity profiles. There continues to be disagreement about whether multiple similarity states are possible in the plane wake, with Narasimha (1989) and Sreenivasan & Narasimha (1982) arguing that the growth-rate differences observed by Wygnanski *et al.* (1986) and others are long-lived transients. Because the time period that can be simulated computationally is limited, we will be unable to definitively settle this issue here.

The evolution of large-scale coherent structures in the plane wake has been of great interest (e.g. Antonia, Browne & Bissett 1987; Hayakawa & Hussain 1989). Part of the reason for this interest is that the well-known features of transitional wakes, such as the Kármán street, have been observed in the turbulent wake as well. George (1989) argued that the differences between the asymptotic states in the far field of the wake could arise from persistence of different large-scale structures from the near field into the far field of the wake. However, the extent to which such structures are dynamically important in the far field and how they vary among different wakes is not, as yet, well understood. For example, the level of the 'two-dimensionality' that occurs in developed free-shear flows has been widely debated, with some researchers claiming that the relatively organized large-scale structures will ultimately break down into more three-dimensional turbulence, leading to a universal asymptotic similarity state. It is thus of interest to determine if wakes can achieve self-similar states with different flow structures. To this end, a complementary study is being pursued to examine if the governing equations for more complex statistical measures of the turbulent structures (in particular the two-point velocity correlation) admit similarity solutions.

The non-uniqueness of the approximate similarity states provides both complications and opportunities. It complicates the prediction of the flow using turbulence models since it is necessary to ensure that the model allows for multiple asymptotic states. The non-uniqueness of the flow, though, suggests that it should be possible to control the evolution of the wake by manipulation of the generating body. Progress in both of these areas will be facilitated by knowledge of how the differences in the statistical measures and structures of the far wake are related to differences in the initial state of the wake. Direct numerical simulation is an ideal tool for providing this information because it allows the precise prescription of the initial/inlet conditions and also provides very detailed information about the flow. Three such simulations with differing initial conditions are reported here. The results of the simulations are used in conjunction with a similarity analysis following the approach outlined by George (1989) to examine the differences between the 'equilibrium' states of the three flows. The simulations are described in §2, details of the self-similar analysis and statistical

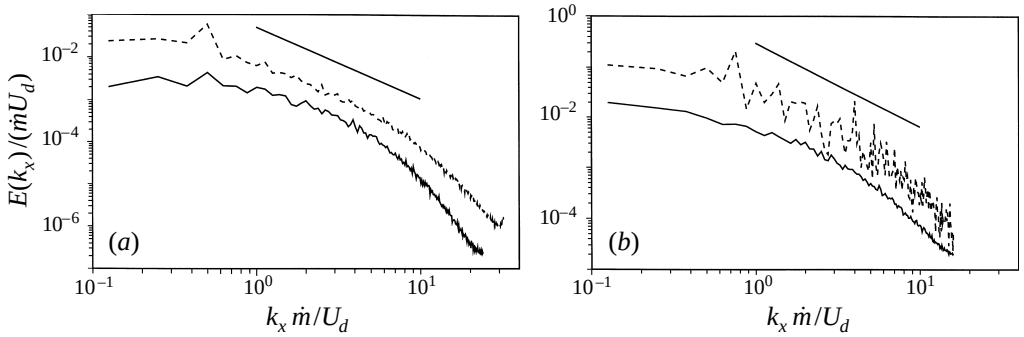

FIGURE 1. Streamwise one-dimensional energy spectra in the ——— unforced wake simulation and the – – – – strongly forced wake simulation at (*a*) the wake centreline, $y = 0$, in the self-similar period ($\tau = tU_d^2/\dot{m} = 91.5$ for the unforced case and $\tau = 50.0$ for the strongly forced case) and (*b*) at the y-location of maximum q^2 at $\tau = 0$. The straight lines show a $k^{-5/3}$ dependence.

descriptions of the three simulated flows are presented in §3, and the structural features of the flows are discussed in §4. Finally, some concluding remarks are given in §5.

2. The simulations

The numerical simulations discussed here were performed by directly solving the three-dimensional time-dependent incompressible Navier–Stokes equations with a Galerkin spectral method (Spalart, Moser & Rogers 1991). However, simulating a wake flow in a computational domain that includes the wake-producing body as well as a long enough streamwise region for the resulting turbulent wake to reach self-similarity is not computationally feasible. Instead, recall that a spatially developing plane wake only approaches self-similarity asymptotically for $|\delta U/U_\infty| \ll 1$, where $\delta U = \overline{U}(y = 0) - U_\infty$ is the centreline wake deficit and U_∞ is the free-stream velocity. Asymptotically, in the same limit, a section of the wake viewed in a reference frame moving at the free-stream velocity appears to be a parallel shear flow evolving in time. Thus, instead of simulating the entire wake and the body generating it, we can simulate a section of the wake by computing such a time-developing flow. Note that the same formulation applies to a jet with coflow (δU positive) provided δU is again small compared to U_∞. We think of the simulations described here as wakes because the initial conditions (see below) are designed to model the turbulent wake of a flat plate.

Formally, the spatially and temporally evolving wakes differ in that different integral quantities are preserved. In the time-developing wake, the cross-stream integrated mass flux deficit (normalized by density and unit depth) $\dot{m} = -\int_{-\infty}^{\infty} \delta U \, \mathrm{d}y$ is preserved, while in the spatially evolving wake, the integrated momentum flux deficit $U_\infty^2\theta = -\int_{-\infty}^{\infty} \delta U(U_\infty + \delta U)\,\mathrm{d}y$ is preserved. However, in the limit of small deficits, the mass flux deficit is given by $\dot{m} = U_\infty\theta$, so in this limit, the same integral quantities are conserved in the spatial and temporal wakes. In the time-developing wake, the free-stream velocity is not dynamically relevant and only the deficit is important. Thus, in what follows, non-dimensionalization will be based on $\dot{m}$ and the initial magnitude of the velocity deficit, U_d. In the three flows described here, the Reynolds number $Re_m = \dot{m}/\nu$ is 2000. This Reynolds number is high enough to produce a short $k^{-5/3}$ spectral range in the streamwise one-dimensional spectrum (figure 1).

The initial conditions for the simulations in this study were generated using two realizations of a turbulent boundary layer computed by Spalart (1988) at a momentum-

thickness Reynolds number of 670. The solution domain for the simulations is periodic in the streamwise (x) and spanwise (z) directions with periods $50\dot{m}/U_d$ and $12.5\dot{m}/U_d$, respectively, to correspond to those in the boundary layer simulations. The streamwise domain length is much larger than the wavelength of the most unstable disturbance to the mean at $t = 0$ and is more than four times that associated with the mean at the start of the self-similar period (see §3.2). Different realizations were used for each side of the wake to avoid any unphysical instantaneous symmetries, and the free-stream velocity on each side was zero. Thus, the simulations represent a temporally evolving approximation to the wake behind a zero-thickness flat plate at zero angle of attack moving at velocity U_d with turbulent boundary layers.

To study the variability of plane wakes and their dependence on initial/upstream conditions, the initial conditions described above were modified in two of the three simulations presented here. To design appropriate modifications, we noted that several experimental observations suggest that two-dimensional or nearly two-dimensional disturbances are important in the evolution of a plane wake. These include the observation of Kármán streets, which are nearly two-dimensional, even in highly turbulent wakes, and the variation of the growth rate with different imposed two-dimensional disturbances, as observed by Wygnanski *et al.* (1986). Furthermore, it is not unreasonable to expect different bodies (e.g. a cylinder and a flat plate) to introduce different two-dimensional disturbances into their wakes because the geometry of the body affects the character of the oscillating, nearly two-dimensional separation that occurs when the wake is generated. Finally, a flat-plate wake can be influenced by acoustic and pressure disturbances that affect the vortical flow through the receptivity of the plate's trailing edge. Such disturbances are expected to have large spanwise wavelengths and therefore produce nearly two-dimensional fluctuations. Effects such as trailing-edge receptivity and the dynamics of separation from the wake generator are not included in the boundary layer initial conditions described above.

Since the influence and evolution of the nearly two-dimensional disturbances discussed above are not well understood, and since such disturbances are apparently important in turbulent plane wakes, the second and third simulations in this study were designed to investigate the impact of two-dimensional disturbances. To this end, the two-dimensional disturbances in the turbulent boundary layer initial conditions were augmented. This is referred to here as 'forcing'. However, it was necessary to avoid the introduction of highly regular disturbances that might produce unrealistically organized structures in the evolved wake. Therefore, the forcing was introduced by amplifying the streamwise and cross-stream components (u and v) of all the two-dimensional modes in the turbulent boundary layer initial condition, producing an uncontrolled two-dimensional disturbance without a characteristic streamwise wavelength. These two-dimensional motions were amplified by a factor 5 in one case and a factor 20 in the other. The two resulting flows are referred to as 'weakly forced' and 'strongly forced', respectively, in contrast to the 'unforced' case described above, in which no additional disturbances were added to the initial boundary layer turbulence.

In the weakly forced case, the factor 5 increase in the amplitude of the two-dimensional turbulence fluctuations might appear to be a large modification to the initial condition. However, in the boundary layers, the two-dimensional disturbances are so small that multiplying them by a factor 5 does not create a particularly large disturbance. In particular, in the unforced initial conditions, the two-dimensional modes constitute only 1.5% of the turbulent kinetic energy density ($q^2/2$) at the point of maximum q^2. After amplification for the weakly forced initial condition, these modes still account for just 25% of $q^2/2$, and only 0.8% of the total flow energy

(including that associated with the wake deficit). Thus the total energy in the flow has not been significantly increased, and it is not unreasonable to expect that disturbances of this magnitude could be introduced naturally at the trailing edge of the plate, or by the wake body. Another way to gauge the strength of the forcing is by examining its impact on the flow development. For the weakly forced wake, the growth rate is within the range of experimentally observed wake growth rates for wakes with no explicit forcing (see §3.2).

In contrast, the forcing level in the strongly forced flow is large, with the two-dimensional disturbances accounting for 86% of the turbulent kinetic energy and 11% of the total flow energy. Thus in this case significant energy ($0.7\dot{m}U_d$ per unit plan area) has been added to the flow. The streamwise spectra of both the strongly forced initial condition and the unforced initial condition are shown in figure 1(*b*). Note the large magnitude and essentially broad-band nature of the spectrum of the forcing. As a result of the strong forcing, the wake growth rate exceeds that of even the periodically forced wakes of Wygnanski *et al.* (1986). In similar simulations of a mixing layer (Rogers & Moser 1994), the amplification factor 20 was needed to produce a significant change in the flow evolution. The wakes examined here are apparently more sensitive to forcing (perhaps because the shear production of turbulence in the wake decreases significantly as the wake velocity deficit decays, whereas the velocity difference in the mixing layer remains constant). Even the 'weak' forcing was found to significantly affect the wake growth rate, whereas the same level of forcing in the mixing layer had a minimal impact.

To achieve the relatively large Reynolds numbers of the computations, while at the same time maintaining an adequate sample of large-scale eddies in the computational domain, requires significant computational resources. The simulations described here employed grids with up to 25 million modes ($600 \times 260 \times 160$) and required between 220 and 530 Cray YMP C-90 CPU hours each to complete.

3. Self-similarity and statistics

3.1. *Similarity of single-point velocity moments*

The temporally evolving plane wake is statistically homogeneous in both the streamwise and the spanwise directions (i.e. x- and z-directions), so the mean momentum equation in deficit form is given by

$$\frac{\partial \delta U}{\partial t} = -\frac{\partial \overline{uv}}{\partial y} + \nu \frac{\partial^2 \delta U}{\partial y^2} \tag{3.1}$$

where u and v are the streamwise (x) and cross-stream (y) velocity fluctuations respectively, $-\delta U = U_\infty - \overline{U}$ is the deficit velocity, and an overbar signifies the expected value or average. Since it is generally accepted that plane wakes evolve at constant Reynolds number, we anticipate that it will be possible to retain the viscous terms in the analysis. This differs from the conventional approach (cf., Tennekes & Lumley 1972), in which it is assumed that only high-Reynolds-number shear layers can evolve self-similarly. Consistency of the scaling constraints arising from the viscous terms with those from other terms will imply that finite Reynolds number wakes can indeed evolve self-similarly. By integrating (3.1) across the layer, and assuming zero free-stream turbulence, it is confirmed that the mass flux deficit

$$\int_{-\infty}^{\infty} -\delta U \, \mathrm{d}y = \dot{m}, \tag{3.2}$$

is a constant.

It is hypothesized that the mean momentum equations (3.1) and (3.2) for this flow admit similarity solutions where the mean velocity profile and the Reynolds stress are given by

$$\delta U = U_s(t) f(\eta) \tag{3.3}$$

and

$$\overline{uv} = R_s(t) g(\eta), \tag{3.4}$$

where $\eta = y/\delta(t)$ is the similarity coordinate. Here we follow the technique of George (1989), choosing individual scales for each of the moments to avoid the possibility of over-constraining the analysis. In particular, it is not assumed *a priori* that the scale for the Reynolds stress $\overline{uv}$ is U_s^2. This scale is determined instead by the constraints imposed by the equations of motion.

A more general Lie group analysis has been carried out by Oberlack (M. Oberlack, private communication) using the techniques described in Oberlack (1997). Oberlack's analysis produces the same similarity forms used here; thus, the forms developed here are the only possible similarity forms for this flow.

Substituting the hypothesized similarity solutions into equations (3.1) and (3.2) yields

$$\left[\frac{\mathrm{d}U_s}{\mathrm{d}t}\right] f - \left[\frac{U_s}{\delta}\frac{\mathrm{d}\delta}{\mathrm{d}t}\right] \eta \frac{\mathrm{d}f}{\mathrm{d}\eta} = -\left[\frac{R_s}{\delta}\right] \frac{\mathrm{d}g}{\mathrm{d}\eta} + \nu \left[\frac{U_s}{\delta^2}\right] \frac{\mathrm{d}^2 f}{\mathrm{d}\eta^2} \tag{3.5}$$

and

$$[U_s \delta] \int_{-\infty}^{\infty} f(\eta) \mathrm{d}\eta = -\dot{m}. \tag{3.6}$$

The time-dependent portion of each term in (3.5) and (3.6) is contained in square brackets (a convention that will be used throughout this similarity analysis). Thus, the hypothesized similarity solutions are consistent with the mean momentum equations if

$$[U_s \delta] \propto \dot{m} \tag{3.7}$$

and

$$\left[\frac{\mathrm{d}U_s}{\mathrm{d}t}\right] \propto \left[\frac{U_s}{\delta}\frac{\mathrm{d}\delta}{\mathrm{d}t}\right] \propto \left[\frac{R_s}{\delta}\right] \propto \left[\frac{U_s}{\delta^2}\right], \tag{3.8}$$

assuming, of course, that none of these terms is zero or negligible. It is straightforward to demonstrate that these constraints are only satisfied when

$$U_s \propto \frac{1}{\delta}, \tag{3.9}$$

$$\frac{\mathrm{d}\delta^2}{\mathrm{d}t} = \text{constant}, \tag{3.10}$$

and

$$R_s \propto U_s \frac{\mathrm{d}\delta}{\mathrm{d}t}. \tag{3.11}$$

Thus, when the flow evolves in a manner consistent with a similarity solution, it follows that

$$\delta \propto (t - t_o)^{1/2}, \quad U_s \propto (t - t_o)^{-1/2} \quad \text{and} \quad R_s \propto (t - t_o)^{-1}, \tag{3.12}$$

where t_o is some virtual origin. Note that it was the viscous term that imposed the constraint leading to (3.10). If the viscous term were neglected (i.e. infinite Reynolds number), the growth of the layer would be undetermined at this point.

Following the methodology outlined by George (1994), the similarity analysis can also be applied to the equations governing the evolution of the individual Reynolds stress components. The transport equations for Reynolds stress components in the temporally evolving plane wake are given by

$$\frac{\partial \overline{u^2}}{\partial t} = -2\overline{uv}\frac{\partial \delta U}{\partial y} - \frac{\partial \overline{u^2 v}}{\partial y} + 2\overline{\frac{p}{\rho}\frac{\partial u}{\partial x}} + \nu\frac{\partial^2 \overline{u^2}}{\partial y^2} - \epsilon_{uu}, \tag{3.13a}$$

$$\frac{\partial \overline{v^2}}{\partial t} = -\frac{\partial \overline{v^3}}{\partial y} + 2\overline{\frac{p}{\rho}\frac{\partial v}{\partial y}} - \frac{2}{\rho}\frac{\partial \overline{pv}}{\partial y} + \nu\frac{\partial^2 \overline{v^2}}{\partial y^2} - \epsilon_{vv}, \tag{3.13b}$$

$$\frac{\partial \overline{w^2}}{\partial t} = -\frac{\partial \overline{w^2 v}}{\partial y} + 2\overline{\frac{p}{\rho}\frac{\partial w}{\partial z}} + \nu\frac{\partial^2 \overline{w^2}}{\partial y^2} - \epsilon_{ww}, \tag{3.13c}$$

and

$$\frac{\partial \overline{uv}}{\partial t} = -\overline{v^2}\frac{\partial \delta U}{\partial y} - \frac{\partial \overline{uv^2}}{\partial y} + \overline{\frac{p}{\rho}\left(\frac{\partial u}{\partial y} + \frac{\partial v}{\partial x}\right)} - \frac{1}{\rho}\frac{\partial \overline{pu}}{\partial y} + \nu\frac{\partial^2 \overline{uv}}{\partial y^2} - \epsilon_{uv}, \tag{3.13d}$$

where p is the fluctuating pressure, ρ is the density, and ϵ_{ij} are the dissipation-rate terms $2\nu\overline{(\partial u_i/\partial x_l)(\partial u_j/\partial x_l)}$. For example, ϵ_{uu} is given by

$$\epsilon_{uu} = 2\nu\left\{\overline{\left(\frac{\partial u}{\partial x}\right)^2} + \overline{\left(\frac{\partial u}{\partial y}\right)^2} + \overline{\left(\frac{\partial u}{\partial z}\right)^2}\right\}. \tag{3.14}$$

Finally, due to incompressibility, the pressure–strain terms in the normal stress equations must sum to zero

$$\overline{\frac{p}{\rho}\frac{\partial u}{\partial x}} + \overline{\frac{p}{\rho}\frac{\partial v}{\partial y}} + \overline{\frac{p}{\rho}\frac{\partial w}{\partial z}} = 0. \tag{3.15}$$

As was done for the mean equation, it is hypothesized that similarity solutions exist for the new moments in the Reynolds stress equations. For example, in the $\overline{u^2}$ equation the solutions are

$$\overline{u^2} = K_u(t)k_u(\eta), \tag{3.16a}$$

$$\overline{u^2 v} = Tt_u(t)tt_u(\eta), \tag{3.16b}$$

$$\overline{\frac{p}{\rho}\frac{\partial u}{\partial x}} = \Pi_u(t)\pi_u(\eta), \tag{3.16c}$$

and

$$\epsilon_{uu} = D_u(t)d_u(\eta). \tag{3.16d}$$

The assumed solutions for the other terms in the equations are given in the second column of table 1.

Substituting the hypothesized forms of the similarity solutions (and those defined previously) into (3.13) yields

$$\left[\frac{\mathrm{d}K_u}{\mathrm{d}t}\right]k_u - \left[\frac{K_u}{\delta}\frac{\mathrm{d}\delta}{\mathrm{d}t}\right]\eta\frac{\mathrm{d}k_u}{\mathrm{d}\eta} = -2\left[\frac{R_s U_s}{\delta}\right]g\frac{\mathrm{d}f}{\mathrm{d}\eta} - \left[\frac{Tt_u}{\delta}\right]\frac{\mathrm{d}tt_u}{\mathrm{d}\eta} + 2\left[\Pi_u\right]\pi_u + \nu\left[\frac{K_u}{\delta^2}\right]\frac{\mathrm{d}^2 k_u}{\mathrm{d}\eta^2} - \left[D_u\right]d_u, \tag{3.17}$$

where again the time-dependent portion of each term is contained in square brackets.

Term	Form	Similarity conditions	Scaling for (3.25)
δU	$U_s(t)f(\eta)$	$U_s \propto \frac{1}{\delta}$	
$\overline{u^2}$	$K_u(t)k_u(\eta)$	$K_u \propto U_s^2$	$K_u = U_s^2\beta$
$\overline{v^2}$	$K_v(t)k_v(\eta)$	$K_v \propto U_s^2$	$K_v = U_s^2\beta^2$
$\overline{w^2}$	$K_w(t)k_w(\eta)$	$K_w \propto U_s^2$	$K_w = U_s^2\beta$
$\overline{uv}$	$R_s(t)g(\eta)$	$R_s \propto U_s\frac{\mathrm{d}\delta}{\mathrm{d}t}$	$R_s = U_s^2\beta$
$\overline{\frac{p}{\rho}\frac{\partial u}{\partial x}}$	$\Pi_u(t)\pi_u(\eta)$	$\Pi_u \propto \frac{U_s^2}{\delta}\frac{\mathrm{d}\delta}{\mathrm{d}t}$	$\Pi_u = \frac{U_s^3\beta^2}{\delta}$
$\overline{\frac{p}{\rho}\frac{\partial v}{\partial y}}$	$\Pi_v(t)\pi_v(\eta)$	$\Pi_v \propto \frac{U_s^2}{\delta}\frac{\mathrm{d}\delta}{\mathrm{d}t}$	$\Pi_v = \frac{U_s^3\beta^2}{\delta}$
$\overline{\frac{p}{\rho}\frac{\partial w}{\partial z}}$	$\Pi_w(t)\pi_w(\eta)$	$\Pi_w \propto \frac{U_s^2}{\delta}\frac{\mathrm{d}\delta}{\mathrm{d}t}$	$\Pi_w = \frac{U_s^3\beta^2}{\delta}$
$\overline{\frac{p}{\rho}\left(\frac{\partial u}{\partial y}+\frac{\partial v}{\partial x}\right)}$	$\Pi_{uv}(t)\pi_{uv}(\eta)$	$\Pi_{uv} \propto \frac{U_s}{\delta}\left(\frac{\mathrm{d}\delta}{\mathrm{d}t}\right)^2$	$\Pi_{uv} = \frac{U_s^3\beta^2}{\delta}$
$\overline{u^2v}$	$Tt_u(t)tt_u(\eta)$	$Tt_u \propto U_s^2\frac{\mathrm{d}\delta}{\mathrm{d}t}$	$Tt_u = U_s^3\beta^2$
$\overline{v^3}$	$Tt_v(t)tt_v(\eta)$	$Tt_v \propto U_s^2\frac{\mathrm{d}\delta}{\mathrm{d}t}$	$Tt_v = U_s^3\beta^3$
$\overline{w^2v}$	$Tt_w(t)tt_w(\eta)$	$Tt_w \propto U_s^2\frac{\mathrm{d}\delta}{\mathrm{d}t}$	$Tt_w = U_s^3\beta^2$
$\overline{uv^2}$	$Tt_{uv}(t)tt_{uv}(\eta)$	$Tt_{uv} \propto U_s\left(\frac{\mathrm{d}\delta}{\mathrm{d}t}\right)^2$	$Tt_{uv} = U_s^3\beta^2$
$\frac{\overline{pv}}{\rho}$	$Pt_v(t)pt_v(\eta)$	$Pt_v \propto U_s^2\frac{\mathrm{d}\delta}{\mathrm{d}t}$	$Pt_v = U_s^3\beta^3$
$\frac{\overline{pu}}{\rho}$	$Pt_{uv}(t)pt_{uv}(\eta)$	$Pt_{uv} \propto U_s\left(\frac{\mathrm{d}\delta}{\mathrm{d}t}\right)^2$	$Pt_{uv} = U_s^3\beta^3$
ϵ_{uu}	$D_u(t)d_u(\eta)$	$D_u \propto \frac{U_s^2}{\delta}\frac{\mathrm{d}\delta}{\mathrm{d}t}$	$D_u = \frac{U_s^3\beta^2}{\delta}$
ϵ_{vv}	$D_v(t)d_v(\eta)$	$D_v \propto \frac{U_s^2}{\delta}\frac{\mathrm{d}\delta}{\mathrm{d}t}$	$D_v = \frac{U_s^3\beta^2}{\delta}$
ϵ_{ww}	$D_w(t)d_w(\eta)$	$D_w \propto \frac{U_s^2}{\delta}\frac{\mathrm{d}\delta}{\mathrm{d}t}$	$D_w = \frac{U_s^3\beta^2}{\delta}$
ϵ_{uv}	$D_{uv}(t)d_{uv}(\eta)$	$D_{uv} \propto \frac{U_s^2}{\delta}\frac{\mathrm{d}\delta}{\mathrm{d}t}$	$D_{uv} = \frac{U_s^3\beta}{\delta}$

TABLE 1. Similarity forms for terms in the mean and Reynolds stress equations

The other equations are analogous. If the time-dependence of the coefficients in brackets is identical, then the equations admit similarity solutions of the form given in table 1. Thus for a similarity solution, it is sufficient that

$$\left[\frac{\mathrm{d}K_u}{\mathrm{d}t}\right] \propto \left[\frac{K_u}{\delta}\frac{\mathrm{d}\delta}{\mathrm{d}t}\right] \propto \left[\frac{R_s U_s}{\delta}\right] \propto \left[\frac{T t_u}{\delta}\right] \propto [\Pi_u] \propto \left[\frac{K_u}{\delta^2}\right] \propto [D_u], \tag{3.18a}$$

$$\left[\frac{\mathrm{d}K_v}{\mathrm{d}t}\right] \propto \left[\frac{K_v}{\delta}\frac{\mathrm{d}\delta}{\mathrm{d}t}\right] \propto \left[\frac{T t_v}{\delta}\right] \propto [\Pi_v] \propto \left[\frac{P t_v}{\delta}\right] \propto \left[\frac{K_v}{\delta^2}\right] \propto [D_v], \tag{3.18b}$$

$$\left[\frac{\mathrm{d}K_w}{\mathrm{d}t}\right] \propto \left[\frac{K_w}{\delta}\frac{\mathrm{d}\delta}{\mathrm{d}t}\right] \propto \left[\frac{T t_w}{\delta}\right] \propto [\Pi_w] \propto \left[\frac{K_w}{\delta^2}\right] \propto [D_w], \tag{3.18c}$$

$$\left[\frac{\mathrm{d}R_s}{\mathrm{d}t}\right] \propto \left[\frac{R_s}{\delta}\frac{\mathrm{d}\delta}{\mathrm{d}t}\right] \propto \left[\frac{K_v U_s}{\delta}\right] \propto \left[\frac{T t_{uv}}{\delta}\right] \propto [\Pi_{uv}] \propto \left[\frac{P t_{uv}}{\delta}\right] \propto \left[\frac{R_s}{\delta^2}\right] \propto [D_{uv}], \tag{3.18d}$$

and

$$[\Pi_u] \propto [\Pi_v] \propto [\Pi_w], \tag{3.18e}$$

where the last condition arises from the requirement that the pressure–strain terms sum to zero, (3.15). Although the conditions (3.18*a*)–(3.18*e*) are sufficient for self-similarity they are not necessary. In theory, groups of terms in the equations could balance and scale independently. However, without any further physical insight as to why this might happen (and for which groups of terms), these solutions could only be found using empirical techniques.

It is clear that the constraints in (3.18*a*) are satisfied if the scales for the terms in the normal stress $\overline{u^2}$ equation are chosen such that

$$K_u \propto U_s^2, \tag{3.19}$$

$$T t_u \propto U_s^2 \frac{\mathrm{d}\delta}{\mathrm{d}t}, \tag{3.20}$$

and

$$\Pi_u \propto D_u \propto \frac{U_s^2}{\delta}\frac{\mathrm{d}\delta}{\mathrm{d}t}. \tag{3.21}$$

Similarly, the other Reynolds stress transport equations admit self-similar solutions when the scales are given as in the third column of table 1. Note that the similarity conditions for the Reynolds shear stress equation (3.18*d*) and the scalings in table 1 require that

$$\left[\frac{R_s}{\delta}\frac{\mathrm{d}\delta}{\mathrm{d}t}\right] \propto \left[\frac{K_v U_s}{\delta}\right] \Rightarrow \left(\frac{\mathrm{d}\delta}{\mathrm{d}t}\right)^2 \propto U_s^2, \tag{3.22}$$

which using (3.9) implies that

$$\frac{\mathrm{d}\delta^2}{\mathrm{d}t} = \text{constant}, \tag{3.23}$$

in agreement with the result from the analysis of the mean momentum equation (3.10). Thus, the constraints imposed by retaining the viscous terms in the momentum equation are consistent with those deduced from the equations for the Reynolds stresses, indicating that self-similar solutions can exist for wakes at all Reynolds numbers.

The similarity requirements outlined above only require that the time-dependent portions of the solutions are proportional to the given scales. As George (1989)

argued, the value of the constants of proportionality may depend on the initial (or source) conditions of the flow. This dependence is expressed in terms of a number of non-dimensional constants. The most important, in this case, is the ratio of the two different velocity scales used in the analysis: U_s, a convective velocity scale, and $\mathrm{d}\delta/\mathrm{d}t$, a characteristic velocity scale for the growth rate of the layer. This ratio

$$\beta = \frac{1}{U_s}\frac{\mathrm{d}\delta}{\mathrm{d}t} = \frac{1}{2U_s\delta}\frac{\mathrm{d}\delta^2}{\mathrm{d}t} = -\frac{\delta}{U_s^2}\frac{\mathrm{d}U_s}{\mathrm{d}t} \tag{3.24}$$

is a constant in a self-similar wake from (3.9) and (3.23) and is a non-dimensional measure of the growth rate of the layer. Note that this ratio can also be interpreted as the ratio of a convective time scale and a time scale characteristic of the spreading rate of the flow. This interpretation is useful in the analysis of the moments involving velocities at two times that will be discussed elsewhere.

For example, using the scaling in the fourth column of table 1, the resulting governing equations for the similarity profiles are given by

$$\int_{-\infty}^{\infty} f(\eta)\mathrm{d}\eta = \frac{-\dot{m}}{U_s\delta}, \tag{3.25a}$$

$$-\frac{\mathrm{d}\eta f}{\mathrm{d}\eta} = -\frac{\mathrm{d}g}{\mathrm{d}\eta} + \frac{1}{Re_\delta\beta}\frac{\mathrm{d}^2 f}{\mathrm{d}\eta^2}, \tag{3.25b}$$

$$-2k_u - \eta\frac{\mathrm{d}k_u}{\mathrm{d}\eta} = -\left\{\frac{1}{\beta}\right\}2g\frac{\mathrm{d}f}{\mathrm{d}\eta} - \frac{\mathrm{d}tt_u}{\mathrm{d}\eta} + 2\pi_u + \frac{1}{Re_\delta\beta}\frac{\mathrm{d}^2 k_u}{\mathrm{d}\eta^2} - d_u, \tag{3.25c}$$

$$-2k_v - \eta\frac{\mathrm{d}k_v}{\mathrm{d}\eta} = -\frac{\mathrm{d}tt_v}{\mathrm{d}\eta} + \left\{\frac{1}{\beta}\right\}2\pi_v - 2\frac{\mathrm{d}pt_v}{\mathrm{d}\eta} + \frac{1}{Re_\delta\beta}\frac{\mathrm{d}^2 k_v}{\mathrm{d}\eta^2} - \left\{\frac{1}{\beta}\right\}d_v, \tag{3.25d}$$

$$-2k_w - \eta\frac{\mathrm{d}k_w}{\mathrm{d}\eta} = -\frac{\mathrm{d}tt_w}{\mathrm{d}\eta} + 2\pi_w + \frac{1}{Re_\delta\beta}\frac{\mathrm{d}^2 k_w}{\mathrm{d}\eta^2} - d_w, \tag{3.25e}$$

$$-2g - \eta\frac{\mathrm{d}g}{\mathrm{d}\eta} = -k_v\frac{\mathrm{d}f}{\mathrm{d}\eta} - \frac{\mathrm{d}tt_{uv}}{\mathrm{d}\eta} + \pi_{uv} - \{\beta\}\frac{\mathrm{d}pt_{uv}}{\mathrm{d}\eta} + \frac{1}{Re_\delta\beta}\frac{\mathrm{d}^2 g}{\mathrm{d}\eta^2} - \left\{\frac{1}{\beta}\right\}d_{uv}, \tag{3.25f}$$

and

$$\pi_u + \pi_v + \pi_w = 0, \tag{3.25g}$$

where $Re_\delta = U_s\delta/\nu$ is the Reynolds number. Note that these equations include only three non-dimensional constants: the shape factor $U_s\delta/\dot{m}$, the Reynolds-number Re_δ and the growth rate β. It is commonly assumed, as in many other turbulent flows, that for large Re_δ, the similarity profiles will become Reynolds-number independent (i.e. there is a regular limit as $Re \to \infty$). Note, however, that equations (3.25) suggest that it is $Re_\delta\beta$, the Reynolds number based on $\mathrm{d}\delta/\mathrm{d}t$ that must be large. It has also been observed that well-developed wakes all have essentially the same mean velocity profile, thus the shape factor $U_s\delta/\dot{m}$ is universal. It is only β that could vary from wake to wake, depending on the details of how it is created or initialized.

Other authors have used different parameters to characterize wake similarity states. In particular, Sreenivasan & Narasimha (1982) used the parameters defined by Prabhu & Narasimha (1972), which in the context of the current time-developing analysis are given by $W = U_s((t-t_0)/\dot{m})^{1/2}$ and $\Delta = \delta((t-t_0)\dot{m})^{1/2}$, where t_0 is a virtual origin for time. It is easily shown that in a self-similar wake, parameterization with W and Δ is equivalent to parameterization with β and $U_s\delta/\dot{m}$, and that

$$\beta = \frac{\Delta}{W} \quad \text{and} \quad \frac{\delta U_s}{\dot{m}} = W\Delta. \tag{3.26}$$

Note that in Prabhu & Narasimha (1972), Δ is defined with δ equal to half the half-width defined in §3.2. The shape factor and β are used here instead because they arise naturally in the above analysis and they do not require explicit determination of t_0. Furthermore, when similarity breaks down, the parameters are not equivalent, and Δ/W is a particularly poor indicator of this breakdown. The assertion of Sreenivasan & Narasimha (1982) that Δ and W are universal is here seen to be equivalent to a statement that β and $U_s\delta/\dot{m}$ are universal. The similarity analysis clearly neither requires or precludes this.

If a scaling could be chosen that would eliminate all the β-dependent coefficients in the profile equations, then the plane wake would admit a family of self-similar states with different growth rates but identical similarity profiles (when properly scaled). However, in this case it is not possible to remove the β coefficients from all of the terms in the stress equations or the pressure–strain balance regardless of what factors of β are chosen for the individual scales. That this is true can be easily seen by considering the following chain of scaling requirements that attempt to eliminate β factors from the equations.

(*a*) No β on the Reynolds stress term in the mean equation implies $R_s \sim U_s^2\beta$.

(*b*) No β on the u^2 production term or the u^2 time derivative term implies $K_u \sim U_s^2$.

(*c*) No β in the balance of the pressure–strain terms implies that all the diagonal pressure–strain scales (i.e. Π_u, Π_v and Π_w) have the same β scaling.

(*d*) No β on the pressure–strain or time-derivative terms in the u^2, v^2, and w^2 equations implies that K_u, K_v, and K_w have the same β factor, and in particular $K_v \sim U_s^2$.

(*e*) No β on the uv time-derivative or uv production terms implies $R_s \sim U_s^2/\beta$.

Item (*e*) contradicts item (*a*), demonstrating that it is not possible to eliminate β factors from the similarity form of the Reynolds stress equations. Furthermore, although the growth rate dependence may only appear in one or a few of the equations, the equations are coupled so the growth-rate dependence can in principle affect all the profiles. As a result, the shape of at least some of the similarity profiles for the single-point moments must differ for wakes with different normalized growth rates.

The most appropriate choice for the scale factors can be found by examining data from wakes with different growth rates. Such wakes *necessarily* have different self-similar profiles, but certain scalings may be able to minimize the differences in the overall magnitude of the profiles. The particular scalings given in the fourth column of table 1 were selected with guidance from the DNS data (§3.2) and represent the scalings that minimize the gross magnitude variations among the profiles for the three simulated wakes. Use of these scalings results in more factors of β in the profile equations than the minimum possible.

Note that scaling the Reynolds shear stress with $U_s^2\beta$ has resulted in a mean velocity equation (3.25*b*) without explicit growth-rate dependence. Thus, if wakes with different growth rates have universal mean velocity profiles as is observed both in experiments (Wygnanski *et al.* 1986) and the current numerical simulations (§3.2), then the Reynolds stress profile scaled in this way must also be universal. Indeed, this was the major motivation for scaling $\overline{uv}$ with $U_s^2\beta$. It is curious that the Reynolds shear stress profile is universal while the $\overline{uv}$ stress equation has explicit β-dependence. Apparently, the non-universality of profiles for the terms of this equation cancel when they are added together. It is possible to choose β scalings that result in no explicit β dependence in the $\overline{uv}$ equation, but these do not agree with the simulation data.

It is evident from the above analysis that the governing equations for the Reynolds stresses in the time-developing wake admit similarity solutions, provided that the

assumed forms of the higher-order quantities (e.g. the pressure–strain terms, the transport terms, and the dissipation) are allowed. It is not possible to verify this in the context of the current analysis due to the closure problem. However, using a more general technique based on Lie groups, Oberlack (1997) has shown that similarity of the second moments for flows with these similarity variables implies similarity of the higher-order quantities. Of course, the analysis only confirms that the solutions are possible and does not imply that they must occur in reality. Thus in order to determine whether the hypothesized solutions are a good description of an actual flow it is necessary to test the predictions of the theory with experimental or simulated flow data.

3.2. *Comparison with the simulations*

In this subsection, the simulations described in §2 are examined to determine whether the similarity described in §3.1 is achieved. Formally the time-developing plane wake can only be self-similar if the streamwise and spanwise domain sizes are infinite. Otherwise, the finite domain size would introduce a physical length scale (other than a characteristic wake thickness), which results in a loss of self-similarity. Of course the simulations performed here have finite streamwise and spanwise domain sizes, which means that if approximate self-similarity is to be achieved, the domain size must be much larger than the largest scales of the turbulence, so that the evolution of the turbulence will not be affected by the finite domain. As the size of the turbulent eddies grows in time, the infinite-domain approximation breaks down and results in the loss of similarity at late times in the simulations. All evidence suggests that this finite domain-size effect is indeed responsible for the eventual loss of similarity observed in all the simulations reported below. During the self-similar period of the simulations, the finite-domain simulation is used as an approximation of the infinite-domain self-similar wake.

In applying the similarity analysis to the simulated wakes, any number of different thickness measures (δ) and velocity scales (U_s) could be used. To facilitate comparison to previous experimental data, we will use the maximum magnitude of the velocity deficit (U_0) and the half-width b, which is defined to be the distance between the y-locations at which the mean velocity is half of U_0 (note that some investigators take the half-width to be half this distance).

Shown in figure 2 is the time evolution of b^2 and U_0^{-2} for all three simulations plotted against the dimensionless time $\tau = tU_d^2/\dot{m}$. Both these quantities should evolve linearly during the self-similar period as required by (3.9) and (3.10), and indeed in the unforced and weakly forced flows both have substantial periods of linear growth. The growth rate can be characterized by the non-dimensional growth, β (see §3.1), which when based on U_0 and b is given by

$$\beta = \frac{1}{U_0}\frac{\mathrm{d}b}{\mathrm{d}t}. \tag{3.27}$$

In the unforced and weakly forced flows, $\beta = 0.12$ and 0.21, respectively, during the self-similar period. The analogous growth rate parameter in a spatially developing wake is $\beta = (U_\infty/U_0)(\mathrm{d}b/\mathrm{d}x)$, which was 0.18 in the experiments of Weygandt & Mehta (1995) and ranged from 0.15 to 0.21 in the unforced experiments of Wygnanski *et al.* (1986). Thus the unforced and weakly forced growth rates cover the range of these experimental growth rates for 'natural' wakes. The marked effect of the forcing on the growth rate suggests an explanation for the low growth rate of the unforced case compared to the experiments: it seems likely that the initial conditions for the

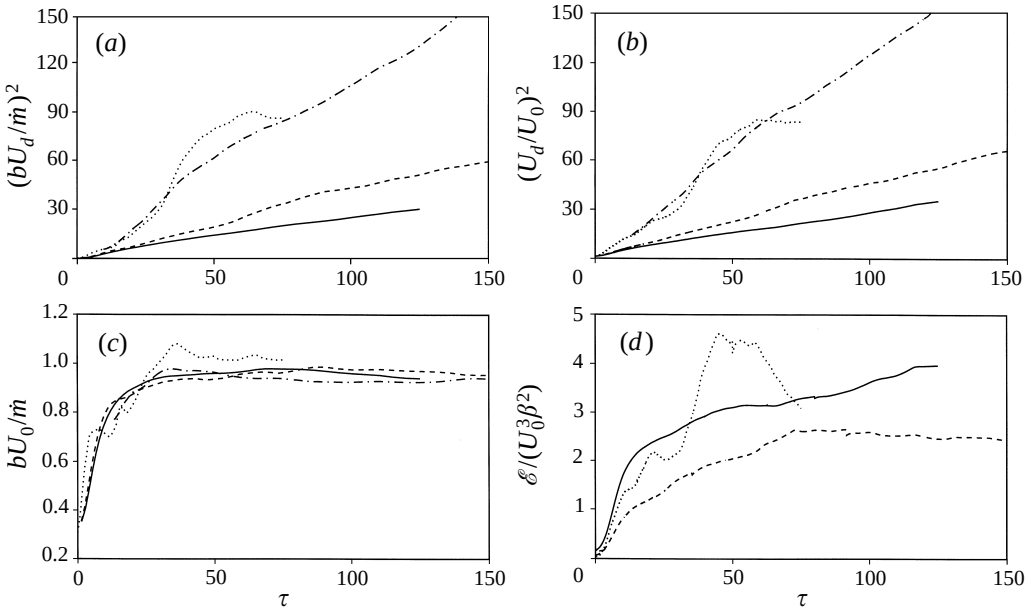

FIGURE 2. Evolution of (*a*) $(bU_d/\dot{m})^2$, (*b*) $(U_d/U_0)^2$, (*c*) $bU_0/\dot{m}$, and (*d*) $\mathscr{E}/(U_0^3\beta^2)$ in the ———, unforced; – – – –, weakly forced; ·····, strongly forced DNS; and —·—, strongly forced LES wake simulations. The strongly forced LES was performed by Ghosal & Rogers (1997) in a spatial domain that is four times larger than the DNS in the spanwise direction and twice as large in the streamwise direction.

unforced case have less large-scale, nearly two-dimensional disturbance energy than is present in most experiments. As discussed in §2, this is expected due to the absence of a splitter plate tip (or other wake generator) in the time-developing simulations.

Unlike the other two cases, the strongly forced case has no extended period of self-similar growth, although there are short periods during which b^2 and/or U_0^{-2} vary linearly. The period that most closely approaches self-similarity in the strongly forced case occurs from about $\tau = 40$ to $\tau = 58$. Here bU_0 (figure 2*c*) appears to be reaching a plateau, indicating that b and U_0 are evolving together. At this time, $\beta = 0.58$, which is larger than the highest forced growth rate observed by Wygnanski *et al.* (1986) ($\beta = 0.29$). Furthermore, it is only during this period that the statistical profiles discussed below are roughly consistent with self-similarity.

Finally, it is likely that the reason the similarity period ends in these flows is that the turbulence structures become too large for the finite spatial domain. To test this hypothesis, Ghosal & Rogers (1997) performed a large-eddy simulation (LES) of the strongly forced wake in a much larger spatial domain. The results of this simulation are also shown in figure 2. Due to the impossibility of using identical initial conditions and the uncertainties of LES, some departure from the small-domain DNS is expected, even at early times when the domain size is not an issue. However, it is remarkable that the LES exhibits an extended period of apparent self-similarity with approximately the same growth rate as that identified during the 'similarity period' of the strongly forced DNS.

Another global quantity that can be examined for evidence of self-similarity is

$$\mathscr{E} = \int_{-\infty}^{\infty} \epsilon \, \mathrm{d}y = \int_{-\infty}^{\infty} \tfrac{1}{2}(\epsilon_{uu} + \epsilon_{vv} + \epsilon_{ww}) \, \mathrm{d}y, \tag{3.28}$$

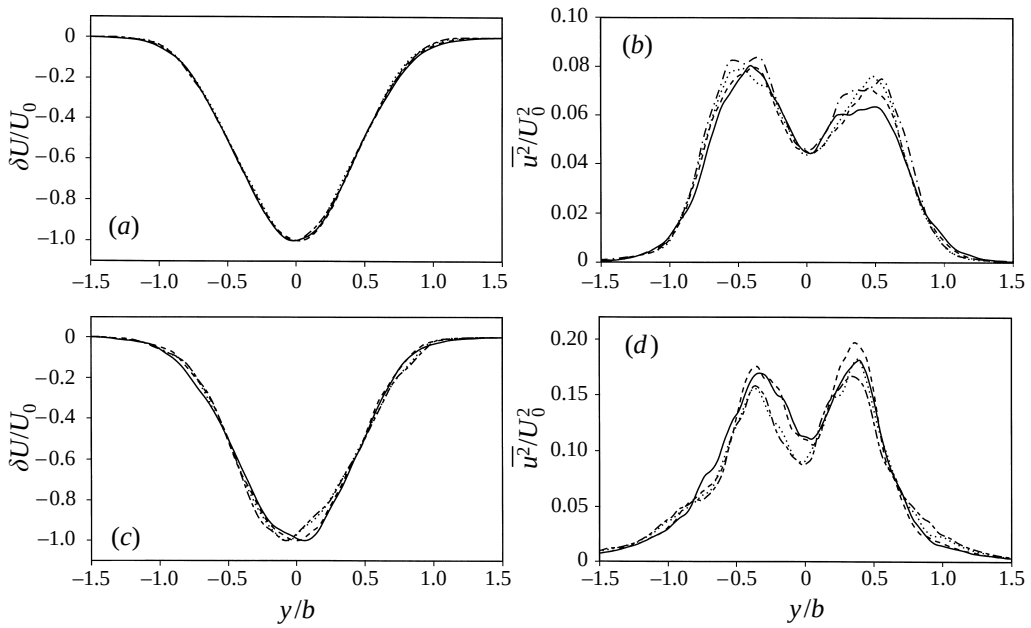

FIGURE 3. Collapse of $\delta U/U_0$ in the (*a*) unforced and (*c*) weakly forced wakes, and $\overline{u^2}/U_0^2$ in the (*b*) unforced and (*d*) weakly forced wakes, in scaled coordinates at four times during the self-similar period. Profiles from the unforced and weakly forced wakes were taken at ———, $\tau = 42.8$ and 64.6; – – – –, $\tau = 56.6$ and 83.1; ·····, $\tau = 71.7$ and 105.6; and —·—, $\tau = 91.5$ and 120.9, respectively.

the integrated rate of kinetic energy dissipation ($\epsilon = 2\nu\overline{S_{ij}S_{ij}}$, where S_{ij} is the strain-rate tensor and ν is the kinematic viscosity). Note that because the flow is inhomogeneous in y, $\epsilon \neq (\epsilon_{uu} + \epsilon_{vv} + \epsilon_{ww})/2$. However, the integral relation in equation (3.28) does hold. According to the scaling in table 1, the integrated dissipation rate should scale with $U_0^3\beta^2$. Thus $\mathscr{E}/(U_0^3\beta^2)$ should be a constant during self-similarity. In figure 2(*d*), it is shown that $\mathscr{E}/(U_0^3\beta^2)$ is indeed approximately constant for $40 \leqslant \tau \leqslant 90$ in the unforced case and for $\tau > 65$ in the weakly forced case. There is little evidence of self-similarity in the dissipation-rate evolution in the strongly forced case, although again $\mathscr{E}/(U_0^3\beta^2)$ is approximately constant for $40 < \tau < 60$. This parameter is apparently a very sensitive indicator of similarity, which has not been previously examined due to the inaccessibility of the dissipation from experiments. Note that the scaling with $U_0^3\beta^2$ has eliminated most of the variation in the magnitude of $\mathscr{E}$ among the different wakes. Compare the variation between the curves in figure 2(*d*) to the factor 23 variation of β^2 among the three wakes.

The self-similarity of the unforced and weakly forced flows is further supported by the collapse of the mean velocity and Reynolds stress profiles when plotted in similarity coordinates. Shown in figure 3 are the mean velocity and streamwise velocity variance at four times, approximately equally spaced through the self-similar period, in both the unforced and weakly forced flows. The collapse of these curves in the unforced flow is good. In the weakly forced flow, there is more variation among the curves, especially for the mean velocity. This, however, may be a result of the inadequate statistical sample of the largest scales, which are larger in the forced cases. Profiles from times outside of the self-similar periods (not shown) do not collapse nearly as well. As in the mixing layer simulations in Rogers & Moser (1994), the breakdown of self-similarity at late times appears to occur because the finite size of the computational domain begins to affect the dynamics of the largest scales of

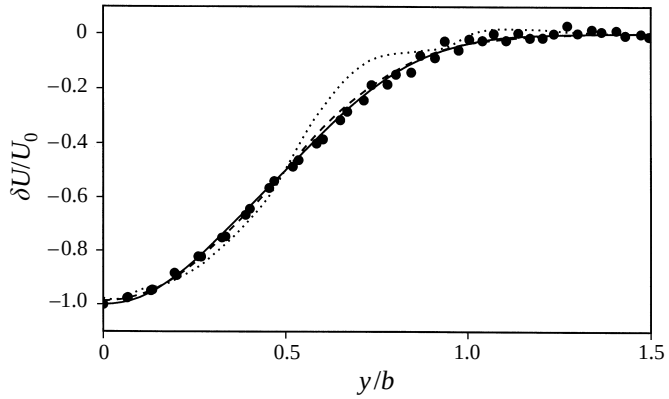

FIGURE 4. Comparison of time-averaged (in scaled coordinates) wake deficit profiles from the ———, unforced; – – – –, weakly forced; and ·····, strongly forced wake simulations, and •, the experiments of Weygandt & Mehta (1995).

motion in the flow. In the strongly forced flow, the mean and variance profiles also collapse fairly well during the brief approximately self-similar period ($40 \leqslant \tau \leqslant 58$).

It is evident from the favourable comparison of the predictions of the hypothesis and the data (especially the collapse of the mean velocity and Reynolds stresses) that the evolution of individual simulations are self-similar during a finite time interval. By examining all the measures of self-similarity presented in this section, especially the collapse of the mean velocity and Reynolds stress profiles discussed above, periods of self-similarity have been defined for each of the three simulated wake flows. For the unforced wake, the period of self-similarity has been determined to be $42.8 < \tau < 91.5$ and the value of β based on the wake growth rate during this period is 0.12. For the weakly forced wake, self-similarity is achieved during $64.5 < \tau < 120.9$ and $\beta = 0.21$. For the strongly forced case, a brief period of approximate self-similarity is found when $39.9 < \tau < 58.3$, during which $\beta = 0.58$. These time intervals are used to generate the time-averaged profiles presented later in this paper. The precisely quoted time limits given above correspond to the times of saved restart files from each simulation. In reality the approach and departure from self-similarity is fairly gradual and deciding which fields are within the self-similar period is somewhat subjective.

3.3. *Comparing different wakes*

Since the statistical quantities collapse in similarity coordinates, they can also be averaged in time over the self-similar period to reduce the statistical noise in the profiles. The profiles from the two sides of the wake are also averaged since they are all statistically symmetric or antisymmetric about the centreline. The results of such averaging are shown in figures 4 and 5 for the mean velocity and Reynolds stress components, respectively. Also shown are the data from Weygandt & Mehta (1995). The Reynolds stress components have been scaled in the conventional way with U_0^2.

The agreement between the mean velocity profiles from the experimental and the unforced and weakly forced computations is very good. However, the mean profile from the strongly forced flow does not agree as well, nor is it as smooth. This is presumably because the simulations provide a poor statistical sample of the large structures that dominate the forced flow (see §4).

As can be seen in figure 5, the conventional scaling of the Reynolds stresses does not collapse the data from various wakes. There is a marked increase in magnitude of

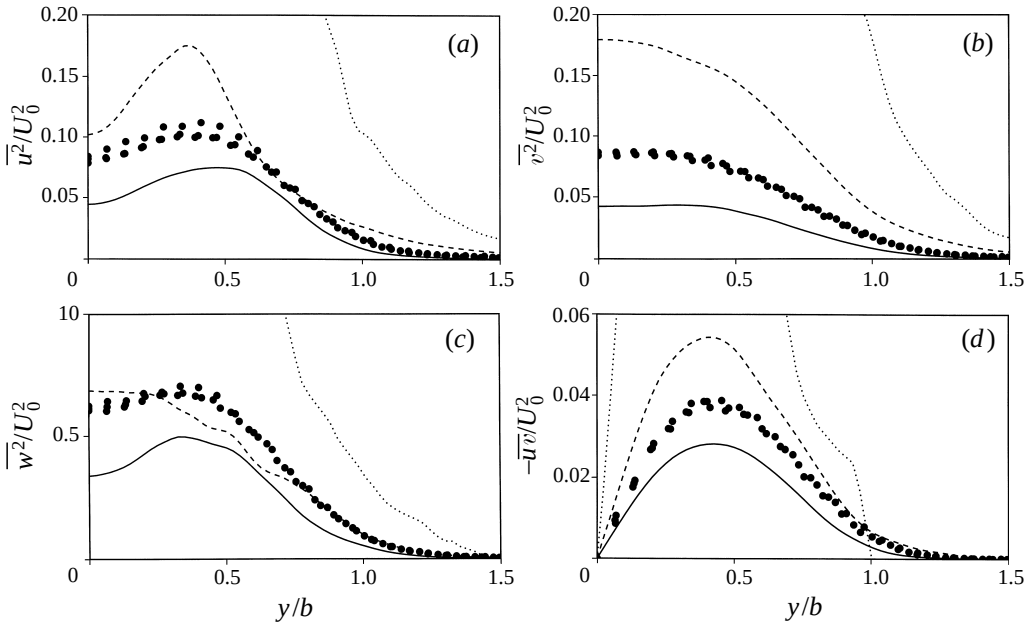

FIGURE 5. Comparison of the time-averaged (in scaled coordinates) components of the Reynolds stress tensor normalized by U_0^2 from the ——, unforced; – – – –, weakly forced; and ·····, strongly forced wake simulations; and •, the experiments of Weygandt & Mehta (1995).

all Reynolds stress components with increasing forcing level, with the experimental data generally falling between the unforced and weakly forced flows. The Reynolds stress levels in the strongly forced case are nearly an order of magnitude larger than those of the unforced case when scaled in this way. Clearly, this common scaling does not allow data from wakes with different growth rates to be effectively compared.

As indicated by the analysis in §3.1, it may be possible to collapse the different Reynolds stress profiles by including factors, or more generally functions, of the dimensionless growth rate β in the scaling. The simulation data can be used to determine the appropriate factors of β to include in the scaling to achieve the best overall collapse of the profiles. By using $U_0^2\beta$ and $U_0^2\beta^2$ to normalize the Reynolds stress profiles, it is possible to obtain approximate collapse of the different wake data, as shown in figure 6. Note that because the self-similarity is less well established in the strongly forced case, less weight should be put on achieving collapse for this case when choosing the appropriate powers of β in the scalings. The selected scalings, which minimize the variation of the similarity profiles among the different wakes, have been listed in the fourth column of table 1.

The choice of the scaling for the Reynolds shear stress is also motivated by the observation that the mean velocity profiles collapse (figure 4), which implies that the shear stress profiles should collapse with the $U_0^2\beta$ scaling (see §3.1). Indeed, in figure 6(*d*), the Reynolds shear stress profiles of the unforced and weakly forced wakes collapse with the experiments from Weygandt & Mehta (1995). The Reynolds stress profile for the strongly forced wake does not collapse as well with the others, which is consistent with the poorer collapse of the mean profile. Note that the scatter between the scaled Reynolds shear stress curves is greater than that among the scaled mean profiles. The viscous terms in the mean momentum equation are indeed small, and this slightly poorer collapse is a result of imperfect self-similarity. For the

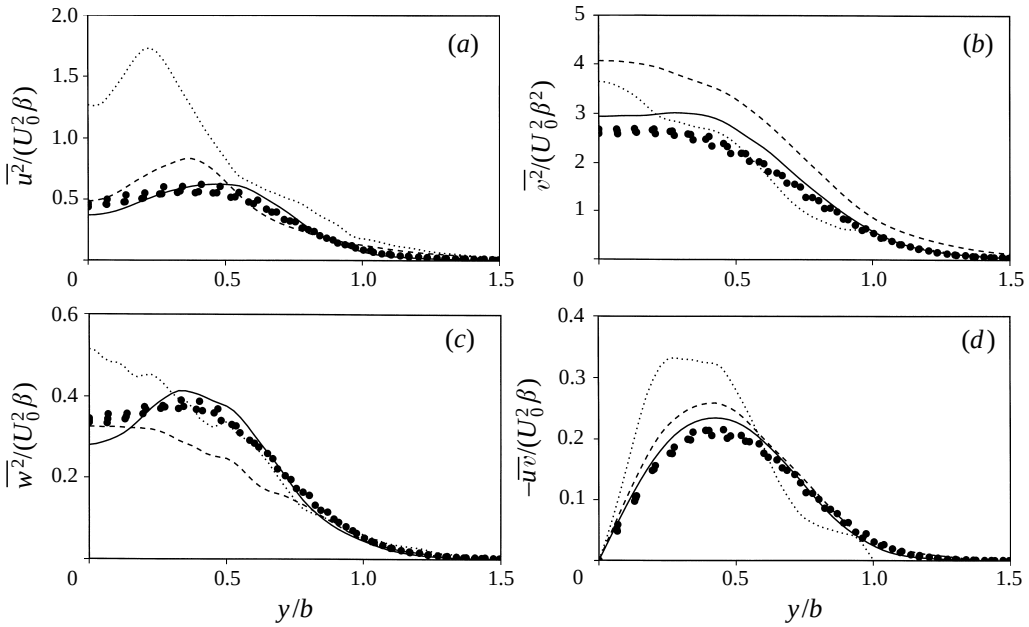

FIGURE 6. Comparison of the time-averaged (in scaled coordinates) profiles of $\overline{u^2}$, $\overline{v^2}$, $\overline{w^2}$, and $\overline{uv}$ normalized by $U_0^2\beta$ ($U_0^2\beta^2$ for $\overline{v^2}$) from the ———, unforced; – – – –, weakly forced; and ·····, strongly forced wake simulations; and •, the experiments of Weygandt & Mehta (1995).

normal stress components, the scaled magnitudes are more or less consistent among the different wakes, but the profile shapes are not. This is to be expected given the growth-rate dependence of the similarity equations (3.25). A similar variation in the shapes of the $\overline{u^2}$ profiles in different wakes was reported in Wygnanski *et al.* (1986).

A similar procedure can be carried out for each of the terms in the Reynolds stress transport equations. Shown in figure 7 are examples of the results of this scaling. Keeping in mind that the goal of the scaling is to eliminate the gross variations in magnitude among the three simulated wakes, it is apparent that the selected growth-rate scaling has succeeded for the $\overline{u^2}$ production and dissipation and the $\overline{v^2}$ pressure–strain (figures 7*a, b* and *c*). This is not surprising for the production since it is just the product of the Reynolds shear stress and the mean velocity gradient, both of which are universal or near universal (see figures 4 and 6 and §3.1). The large peak in the strongly forced curve is due to the poorer collapse of $\overline{uv}$ and δU for the strongly forced case (see figure 6).

The time derivative of $\overline{uv}$ (figure 7*d*), however, is not as well scaled. There is a systematic increase in the magnitude of the curves with forcing level that could be eliminated by scaling with β^3 rather than β^2. But scaling $\overline{uv}$ with β (see table 1) implies the β^2 scaling for the time derivative. In fact, if the $\overline{uv}$ profile is universal as argued previously, then its time derivative should also be universal when scaled with β^2. The poor quality of the scaling for the time derivative suggests a lack of statistical sample and/or imperfect self-similarity in one or more of the simulated wakes (perhaps this is also responsible for the imperfect collapse of the Reynolds shear stress profiles).

In figure 7(*e*), the $\overline{uv}$ pressure diffusion magnitudes have been nicely scaled using $U_0^3\beta^3$, although a β^2 scaling would have been more pleasing as it would have removed

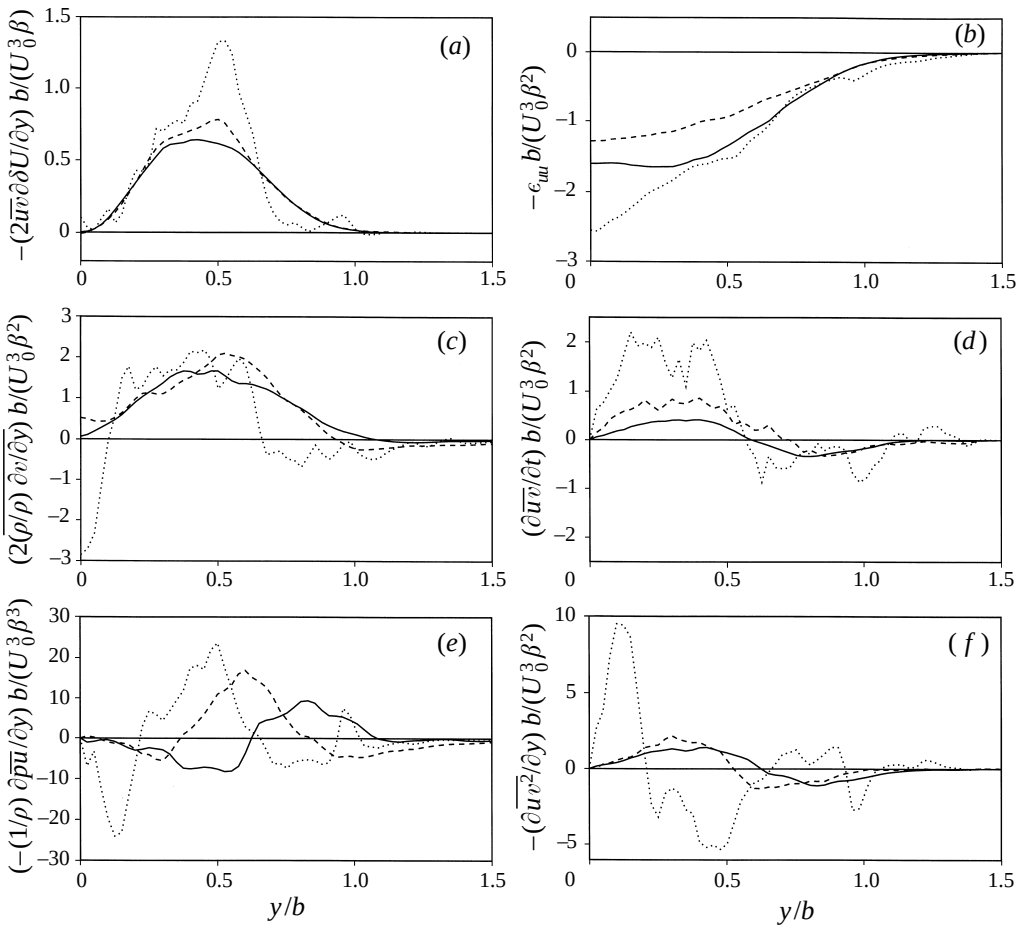

FIGURE 7. Comparison of various terms in the Reynolds stress balance equations from the ———, unforced; – – – –, weakly forced; and ·····, strongly forced wake simulations when scaled as in the fourth column of table 1. Shown are: (*a*) production of $\overline{u^2}$, (*b*) dissipation of $\overline{u^2}$, (*c*) $\overline{v^2}$ pressure–strain term, (*d*) time derivative of $\overline{uv}$, (*e*) pressure diffusion of $\overline{uv}$, and (*f*) turbulent diffusion of $\overline{uv}$.

a β factor from the profile equation (3.25). There is also a large qualitative difference between the pressure diffusion curves and it is not clear what this implies. Finally, examining the turbulent diffusion of $\overline{uv}$ profiles (figure 7*f*), the unforced and weakly forced profiles scale well, and are qualitatively similar. However, the profile from the strongly forced flow is qualitatively different and much larger in magnitude. Since self-similarity in the strongly forced wake is suspect, the scaling for the turbulent diffusion was selected to bring the unforced and weakly forced cases together, without regard to the strongly forced wake. Note that similar plots for the other terms in the Reynolds stress balance have been used to obtain the scalings for these terms, which are summarized in column 4 of table 1 (§2).

3.4. *The role of two-dimensional fluctuations*

As discussed in §2, the difference between the three simulated wakes discussed in this paper is that the 'forced' simulations had amplified two-dimensional fluctuations in the initial conditions. Since this has produced such dramatic differences in the turbulence statistics and particularly the growth rate, the direct contribution of the

two-dimensional fluctuations to the various statistics is of great interest. However, when considering the two-dimensional contribution to a self-similar plane wake a conceptual problem is encountered.

As pointed out in §3.2, the simulations can only model a self-similar time-developing wake of infinite streamwise and spanwise extent if the turbulence scales are significantly smaller than the domain size. It is this difference between the finite-domain computation and the infinite-domain flow that causes a problem in defining the contribution of two-dimensional perturbations. In the computations, the two-dimensional fluctuations are well defined as the average over the spanwise domain, which has length L_z. If L_z is allowed to go to infinity, this average (of the velocity say) will go to zero like $L_z^{-1/2}$ unless there are spanwise-coherent fluctuations with infinite correlation length. In a truly turbulent flow such extreme spanwise coherence is not expected. Even the coherent structures common in free-shear flows become uncorrelated in the span at large enough separations, as suggested by the occurrence of dislocations in such structures as reported by Browand & Troutt (1980). Thus, the contribution of the two-dimensional fluctuations to the energy density or any other quadratic quantity should go to zero like $1/L_z$. Such box-size-dependent measures of two-dimensionality are clearly not useful when investigating the relative importance of spanwise-coherent 'two-dimensional' fluctuations. Indeed, if this subtlety had been fully recognized sooner, the 'forced' initial conditions might have been designed differently.

To address this problem it is necessary to reconsider our intentions in studying 'two-dimensional' fluctuations. In the current context, the interest is in fluctuations with a large spanwise spatial coherence. One way to define such fluctuations would be to apply a spanwise low-pass spatial filter with some filter width L_f; the resulting field would be approximately two-dimensional provided L_f was large compared to the integral scale of the turbulence. The finite-domain spanwise average used in the simulations is an approximation of this, with L_z playing the role of L_f. However, the introduction of a filter width complicates the expected self-similar behaviour of the statistics of the spanwise filtered field. Consider the filtered contribution q_f^2 to q^2 (twice the energy density), which must go like $1/L_f$. Thus, for a self-similar flow, in which the two-point statistics are also similar (Ewing 1995; Ewing *et al.* 1998),

$$q_f^2 \propto \frac{U_0^2 b}{L_f}, \tag{3.29}$$

while the total q^2 evolves like U_0^2. Therefore the ratio q_f^2/q^2 will grow like b, the wake thickness, unless the filter width is also time dependent. Unfortunately, the computational domain width L_z cannot be time dependent. For the spanwise-coherent contribution to be useful in the analysis to follow, such ratios should not evolve in time.

Another way to define the spanwise-coherent fluctuations is as those fluctuations with a spanwise to streamwise aspect ratio (α) greater than some cutoff α_f. This is most easily accomplished by considering the Fourier representation of the velocity in the streamwise and spanwise directions (as is done in the numerical simulations), and defining the spanwise-coherent fluctuations as those associated with Fourier modes with $k_x > \alpha_f k_z$, where k_x and k_z are the streamwise and spanwise wavenumbers, respectively. Since this definition is based on an aspect ratio rather than a filter width, q_c^2/q^2 should be a constant in a self-similar wake (the subscript c denotes the contribution of spanwise-coherent fluctuations defined this way), and the same

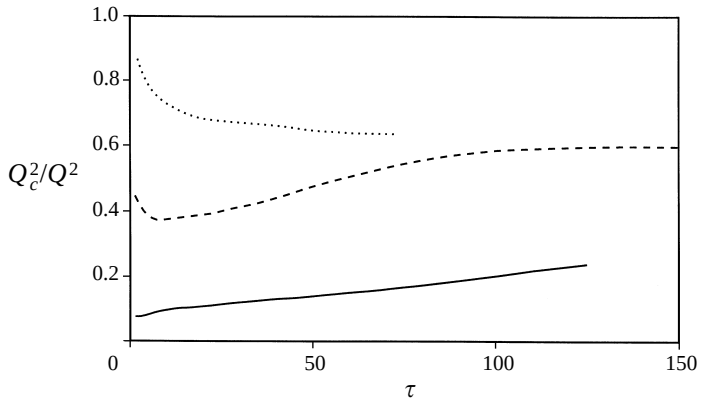

FIGURE 8. Evolution of the ratio of the cross-stream integrated spanwise coherent ($\alpha_f = 4$) contribution q_c^2 to the total cross-stream integrated q^2 in the ———, unforced; – – – –, weakly forced; and ·····, strongly forced wake simulations.

will be true for other quadratic quantities. Because of this desirable property, this aspect ratio definition will be used to study the contribution of spanwise-coherent fluctuations. Several different values for α_f between 2 and 8 have been tried, with little qualitative difference in the results. Thus, only the results with $\alpha_f = 4$ are presented here.

The evolution of the ratio Q_c^2/Q^2, where Q_c^2 and Q^2 are integrals of the coherent and total (respectively) q^2 across the wake, is shown in figure 8 for the three simulations. It is interesting that the proportion of coherent energy continues to rise throughout the self-similar period in the unforced wake, suggesting that the unforced wake is not exactly self-similar after all. In contrast, in the weakly forced wake this ratio does become constant at around $\tau = 100$. For the strongly forced flow Q_c^2/Q^2 appears to be approaching approximately the same value as in the weakly forced flow. It is possible that the unforced flow would also ultimately reach the same value of this ratio, although this is far from certain. Thus, it might be possible that there is a universal value for the ratio of spanwise-coherent energy to total energy (for a given α_f) in a truly self-similar wake. Note that this would not imply that other quantities must be universal, indeed the growth rates and many other quantities as well as the structure (see §4) of the weakly and strongly forced wakes differ.

In both the unforced and weakly forced flows, the Reynolds stress component with the worst collapse is $\overline{v^2}$ (see figure 9*a, c*). Throughout the self-similar period in both flows, there is a monotonic increase of the scaled $\overline{v^2}$ profile. However, when the $\overline{v^2}_c$ contribution is removed (figure 9*b, d*), the curves collapse very well. This is consistent with the Q_c^2/Q^2 evolution for the unforced case. In the weakly forced flow, Q_c^2/Q^2 plateaus only toward the end of the self-similar period as shown in figure 8, and since $\overline{v^2}$ does not dominate q^2, it is possible for this lack of structural self-similarity to be more pronounced in $\overline{v^2}$ than in q^2. In any case, it is clear that the spanwise-coherent fluctuations are not yet completely self-similar in these flows, and this may contribute to a variety of minor inconsistencies in the self-similarity as discussed in the previous sections. It is likely that any lack of similarity in the spanwise-coherent fluctuations is caused by the finite domain size, as an analysis of this data by McIlwain, Ewing & Pollard (1997) indicates that the fluctuations with the largest spanwise scale are responsible.

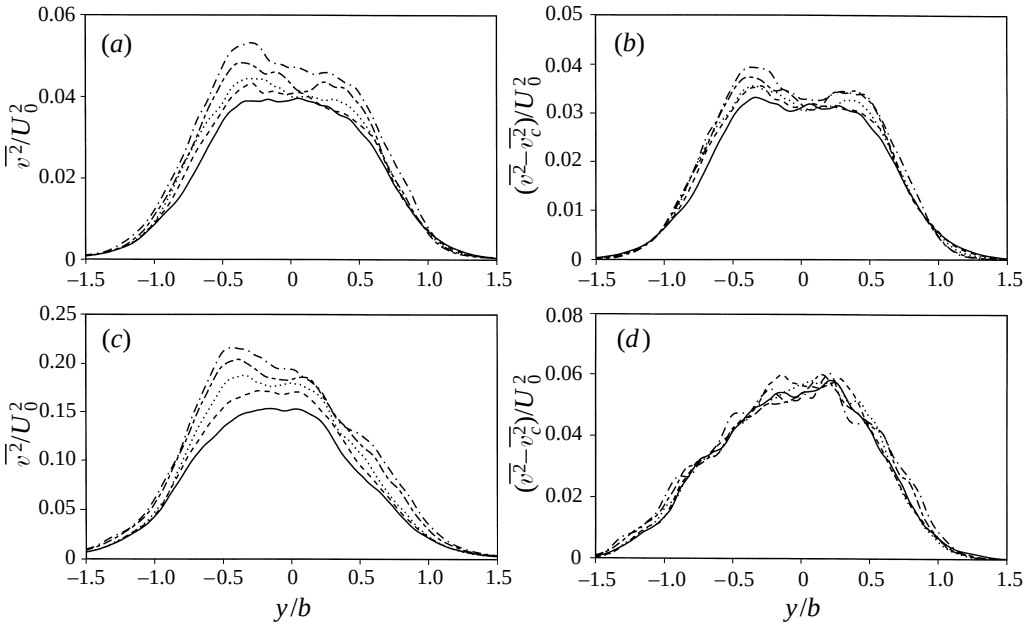

FIGURE 9. Collapse of (*a,c*) $\overline{v^2}/U_0^2$ and (*b,d*) $(\overline{v^2}-\overline{v^2}_c)/U_0^2$ in the (*a,b*) unforced and (*c,d*) weakly forced wakes. Profiles from the unforced and weakly forced wakes were taken at at ———, $\tau = 42.8$ and 64.5; – – – – , $\tau = 51.0$ and 73.6; ····· , $\tau = 62.4$ and 86.6; — – — , $\tau = 74.9$ and 105.6; and — · —, $\tau = 91.5$ and 120.9, respectively.

It was noted in §3.3 that the Reynolds stress components had vastly different magnitudes among the three wakes, and that this could largely be scaled out using the growth rate β. These large differences are at least in part due to the contribution of the spanwise-coherent fluctuations. Shown in figure 10 are the averaged $\overline{u^2}$ and $\overline{v^2}$ profiles (without the β scaling) along with the profiles with the $\overline{u_c^2}$ and $\overline{v_c^2}$ contributions removed. Removing the coherent contribution greatly decreases the variation among the different wakes. In fact, if the selection of the β scaling discussed in §3.1 were based on $\overline{v^2}-\overline{v_c^2}$ a factor of β rather than β^2 would have been chosen. For $\overline{u^2}-\overline{u_c^2}$ and $\overline{w^2}-\overline{w_c^2}$ the best collapse still results from the β scaling used in §3.1, but for $\overline{uv}-\overline{uv}_c$ there are no factors β required to account for magnitude variation among the flows. Thus, much of the non-universality of the self-similar state seems to be linked to the large-scale structures as suggested by George (1989). The fact that the spanwise-incoherent fluctuations (which are expected to dominate the dissipation) yield lower powers of β in the scalings than the total $\overline{v^2}$ and $\overline{uv}$ is probably responsible for the 'inconvenient' scaling of the ϵ_{vv} and ϵ_{uv} terms that result in the $1/\beta$ coefficient appearing on d_v and d_{uv} in (3.25*d*) and (3.25*f*).

3.5. *Other statistics*

In addition to velocity and Reynolds stress statistics, vorticity statistics can be obtained from the simulations. As in Rogers & Moser (1994), the scaling of $\mathscr{E}$ with U_0^3 implies that the vorticity variances should scale like $Re_b U_0^2/b^2$, where $Re_b = U_0 b/\nu$. However, since Re_b is a constant in the self-similar wakes studied here, the Reynolds number factor would only be important when comparing wakes at different Reynolds numbers. As an example, the vorticity variances averaged over the self-similar period in the unforced flow are shown in figure 11. The relative magnitudes of the variances of

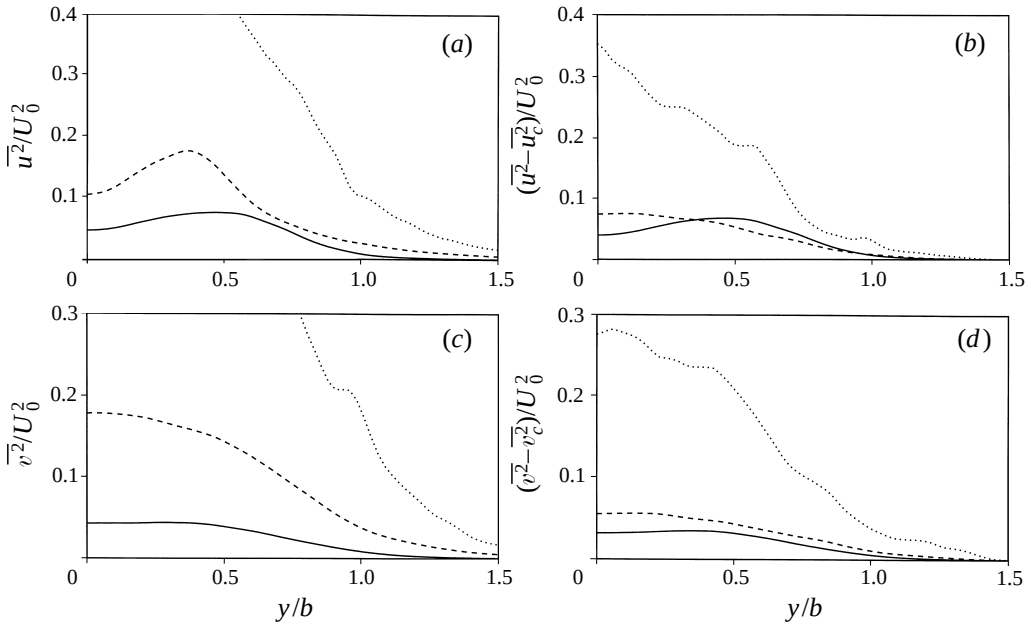

FIGURE 10. Comparison of (*a*) $\overline{u^2}$, (*b*) $\overline{u^2}-\overline{u^2}_c$, (*c*) $\overline{v^2}$ and (*d*) $\overline{v^2}-\overline{v^2}_c$ normalized by U_0^2 from the ———, unforced; – – – –, weakly forced; and ·····, strongly forced wake simulations.

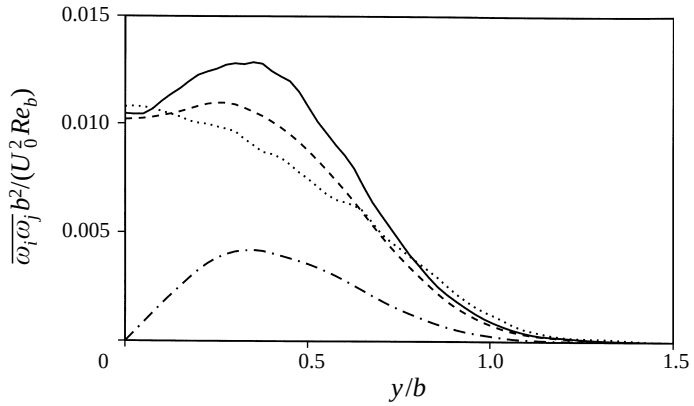

FIGURE 11. Time-averaged (in scaled coordinates) vorticity correlation tensor profiles $\overline{\omega_i\omega_j}$ for the unforced wake: ———, $\overline{\omega_x^2}$; – – – –, $\overline{\omega_y^2}$; ·····, $\overline{\omega_z^2}$; —·—, $\overline{\omega_x\omega_y}$.

the vorticity components are in general agreement with those found in previous computations of homogeneous shear flows (Rogers & Moin 1987) and plane mixing layers (Rogers & Moser 1994).

The time averages of the terms in the balance equation for q^2 over the self-similar periods of the unforced and weakly forced wakes are shown in figure 12. Note that the balances for the individual normal Reynolds stress components and the Reynolds shear stress are given in Appendix A, along with the definitions of the balance terms. The balance for the strongly forced case is not included because the self-similarity in this case is less well established and of short duration. Since the shear is zero at the centre of the wake, the production is zero there. Production of $\overline{q^2}$ thus peaks in the

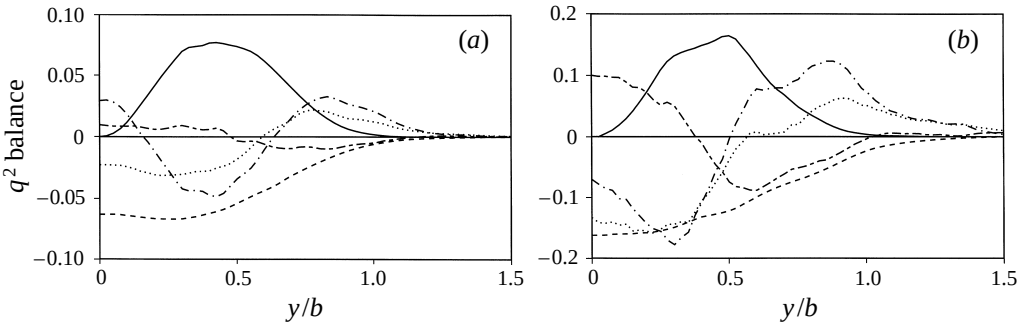

FIGURE 12. Terms in the $\overline{q^2}$ balance equation, scaled by U_0^3/b for (*a*) the unforced wake and (*b*) the weakly forced wake: ———, production; – – – –, dissipation; ·····, time derivative; —·—, turbulent diffusion; and — – —, pressure diffusion.

maximum shear region and $\overline{q^2}$ is transported away by turbulent diffusion. Pressure diffusion provides transport of $\overline{q^2}$ to the centre of the wake, although in the unforced case this transport is rather small and it is the turbulent diffusion that is primarily responsible for transport to the wake centreline. The transport of $\overline{q^2}$ by turbulent diffusion to the edge of the wake causes nearly all of the growth in the width of the $\overline{q^2}$ profile. The negative time derivative near the centre of the wake produces the t^{-1} decay in the maximum $\overline{q^2}$, and the growth in the width of the turbulent region is reflected in the positive time derivative at the edge of the wake. The overall level of the curves in figure 12(*b*) is larger than that in figure 12(*a*) because the increase associated with the larger growth rate β has not been scaled out as it was in in figure 7 (note table 1 indicates that different powers of β are required to compare different terms in the balance).

For a self-similar wake the time derivative can be computed directly from the $\overline{q^2} = U_0^2 h(\eta)$ profile ($\eta = y/b$), with the result

$$\frac{b}{U_0^3}\frac{\partial \overline{q^2}}{\partial t} = -\beta(2h + \eta h'). \tag{3.30}$$

Using the unforced case as an example, at the centreline $h = \overline{q^2}/U_0^2$ is 0.12 and $\beta = 0.12$, resulting in a centreline value of the time derivative of 0.029. This is somewhat larger than the value (0.023) computed from the simulation data and plotted in figure 12. The discrepancy is a measure of the departure of the simulation from self-similarity, and the adequacy of the statistical sample.

Finally, a similarity analysis can also be performed for any passive scalars present in the flow. Such an analysis is presented in Appendix B.

4. Structures

The large statistical differences between the three wakes discussed in §3 are a manifestation of the differences in the structure of the turbulence in these flows. This difference can be seen in figure 13, where spanwise vorticity contours in (x, y)-planes of all three flows are shown. In the strongly forced case, there are concentrations of vorticity fluctuations that occur alternately on one side of the wake or the other, similar to the Kármán street commonly observed in transitional wakes and observed by Wygnanski *et al.* (1986) in the far field of a fully developed wake. By examining other (x, y)-planes (not shown), one can determine that these large-scale features

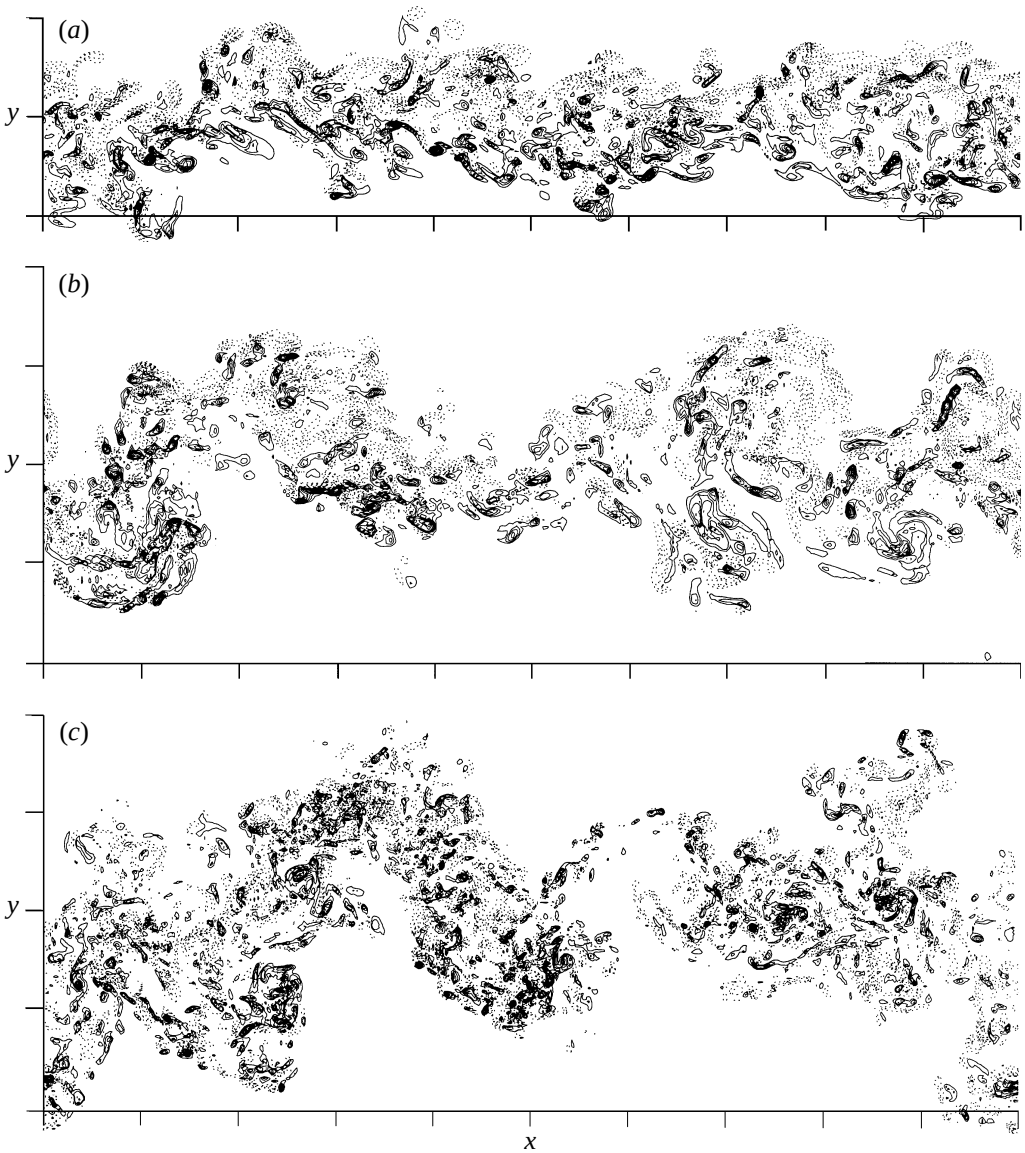

FIGURE 13. Contours of spanwise vorticity in an (x, y)-plane in (a) the unforced flow at $\tau = 91.5$, (b) the weakly forced flow at $\tau = 116$, and (c) the strongly forced flow at $\tau = 50.0$. The contour increments are (a) $2.5U_0/b$, (b) $5U_0/b$ and (c) $20U_0/b$, and negative contours are dotted. Tic marks are at $5\dot{m}/U_d$ intervals.

are spanwise coherent. The vorticity concentrations are also accompanied by large incursions of irrotational fluid into the wake. In contrast, the unforced wake exhibits no such vorticity concentrations, and relatively small incursions of irrotational fluid. It appears to consist of a slab of turbulence with undulating boundaries. The weakly forced flow is intermediate between the other two cases. Forcing was also found to produce large-scale structures similar to those in transitional flows in the turbulent mixing layers of Rogers & Moser (1994).

Another striking difference between the two flows is that the forced flows appear to have vorticity fluctuations of smaller scale, especially the strongly forced flow. This

is consistent with the appearance of the streamwise spatial spectra in figure 1 and the fact that finer spatial resolution was required to compute the forced flow accurately. Comparing figure 13(*a*) and figure 13(*c*), it appears that the strongly forced flow has a larger turbulence Reynolds number than the unforced flow since the ratio of the size of the large-scale features to the size of the small-scale features is greater. Indeed the centreline value of the turbulence Reynolds number $q^4/(\epsilon\nu)$ is an order of magnitude larger in the strongly forced case than in the unforced case ($q^4/(\epsilon\nu) = 4000$, 1500, and 460 for strongly forced, weakly forced, and unforced wakes, respectively) despite the fact that the Reynolds numbers based on $\dot{m}$ are the same in all three flows.

The mixing layer simulations of Rogers & Moser (1994) and Rogers & Moser (1993) suggest that whenever there is a flow region that is dominated by large-scale strain, but largely devoid of (spanwise) vorticity, it is likely that long coherent vortices aligned with the extensional strain (so-called rib vortices), will develop. Such a region might be expected between the vortices in a Kármán street, and indeed rib vortices have been observed in simulations of transitional wakes (Lasheras & Meiburg 1990). A strain-dominated region of this type appears to exist in the forced flow shown in figure 13(*c*) (at $x \approx 30\dot{m}/U_d$), but no rib vortices were found at this time. However, at an earlier time ($\tau = 26.3$, figure 14), the strain-dominated region is also present and rib vortices occur there. The rib vortices can be seen in figure 14(*b*) as the long thin streamwise-oriented regions of large enstrophy at $x \approx 32\dot{m}/U_d$. These vortices span the strain-dominated region, and do not occur elsewhere in the strongly forced flow or anywhere in the weakly forced or unforced flow, which have no such strain-dominated regions. The reason for the disappearance of the rib vortices at later times has not yet been investigated.

5. Conclusions

The evolution of self-similar turbulent plane wakes has been studied using three direct numerical simulations of time-developing wakes. Each simulation was initialized using fields from a previously computed fully developed turbulent boundary layer, thus the simulations are time-developing models for the wake of a flat plate. In addition to the boundary layer turbulence, the energy in the two-dimensional disturbances was augmented in two of the simulations, with the strength of the augmentation differing in the two cases. This was done to mimic the experimental situation in which nearly two-dimensional disturbances can be introduced into the flow as a result of the receptivity of the splitter-plate tip to acoustic disturbances in the facility or by mechanical forcing.

Of the three simulated wakes, the unforced and weakly forced flows exhibit an extended period of self-similarity before the finite computational domain size constrains the flow evolution. In addition, the strongly forced flow has a short period of approximate self-similarity, and the results of recent large-eddy simulations suggest that this self-similar period would endure longer in a larger computational domain (Ghosal & Rogers 1997). While all three flows are at least approximately self-similar, they have markedly different growth rates, turbulence Reynolds numbers, Reynolds stress tensors, and large-scale structures. Thus, consistent with the analysis of the governing equations and experimental observations in several spatially evolving plane wakes, it appears that multiple long-lived self-similar or approximately self-similar states are possible in this flow (if the normalized growth rates differ). Based on the

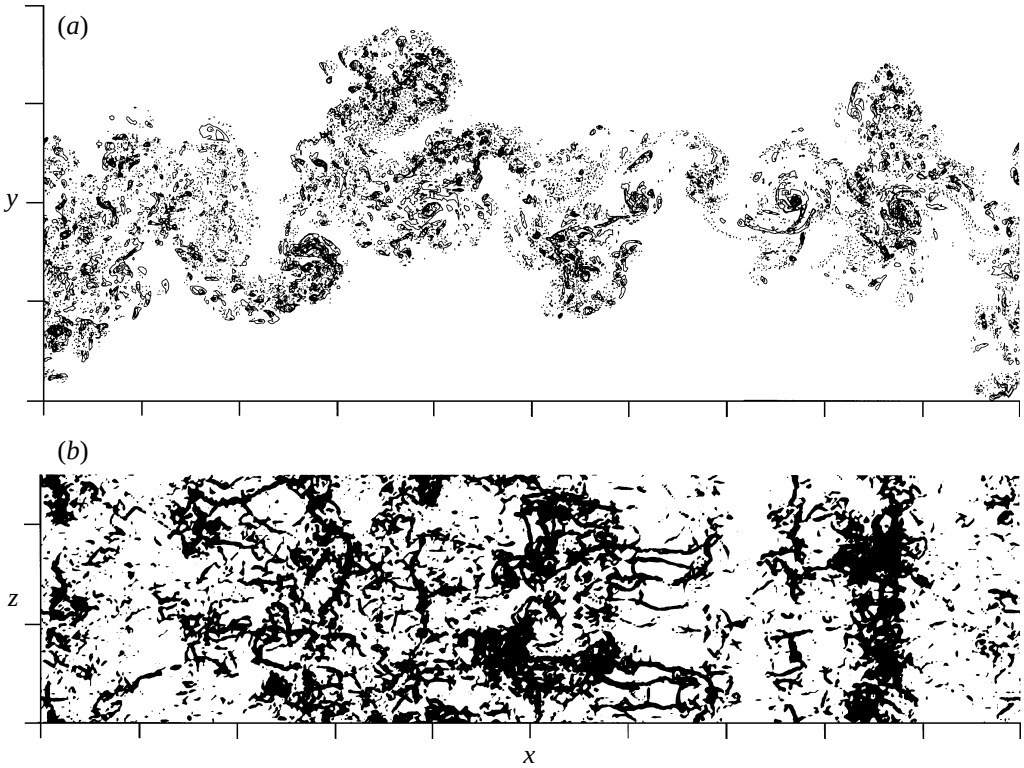

FIGURE 14. (*a*) Contours of spanwise vorticity in an (x, y)-plane (contour increment of $10U_0/b$) and (*b*) top view of regions where enstrophy ($\omega_i\omega_i$) is larger than $8700U_0^2/b^2$ in the strongly forced flow at $\tau = 26.3$. Tic marks are at $5\dot{m}/U_d$ intervals.

current simulations and available experimental data, we cannot definitively determine whether these different similarity states will persist indefinitely.

It is also evident from the analysis of the governing equations for the mean flow and Reynolds stress tensor that the scaling for many of the terms in the equations is ambiguous. This is due to the existence of two velocity scales (the growth rate and the deficit velocity), or equivalently, the existence of an extra parameter (the non-dimensional growth rate parameter β). It was shown that sensible scalings could be found to minimize the differences in the scaled quantities from the different wake flows. The resulting scalings amount to including various factors of β in the conventional scalings based on the velocity deficit.

However, when writing the scaled self-similar Reynolds stress equations using these scalings, factors β appear in the equations. Further, there is no choice of scalings for which factors β are absent. Thus, while plane wakes with different growth rates can be individually *self*-similar, they cannot be dynamically similar to each other. This implies that there is at least a one-parameter family of possible high-Reynolds-number self-similar plane wakes, parameterized by the growth rate (β). Further, the analysis does not *require* that wakes with the same growth rate are similar; it says only that this is allowed. Despite the lack of dynamic similarity, it does appear from both experiments and the current simulations that the mean velocity profile in self-similar plane wakes is universal.

One measure of the structural similarity of the three wakes is the ratio of the energy in the 'spanwise-coherent' fluctuations (defined in §3.4) to the total fluctuation energy.

This ratio should be constant in a self-similar flow, and it is in the weakly forced wake. In the strongly forced wake the ratio is evolving, but appears to be approaching the same value. In the unforced flow, the ratio is smaller but it continues to grow very slowly through the self-similar period. Thus, in this regard the unforced flow is going through a very slow transient as discussed above, although there is no evidence that this is changing the growth rate. This slow increase in the spanwise-coherent energy fraction results in a slight monotonic increase in the scaled cross-stream fluctuation intensity $\overline{v^2}$, which has also been observed in experiments (Weygandt & Mehta 1995). It may be that in truly self-similar wakes, the spanwise-coherent energy ratio is universal or nearly universal. The importance of the coherent fluctuations to the self-similar evolution of the wakes is emphasized by the fact that there is much less variation among the different wakes if only the incoherent fluctuations are included in the statistics.

Over their self-similar periods, the unforced and weakly forced flows exhibit good similarity by the measures generally available from experiments. Yet the slow change in the spanwise-coherent energy measure and other parameters such as the integrated dissipation (figure 2*d*) show that the similarity is not exact. This suggests that self-similarity can also be imperfect in experimental 'self-similar' wakes without being detected. Even in a hypothetical infinitely wide self-similar wake, there could be large spanwise wavelength fluctuations, whose evolution spoils exact structural similarity. It is not unreasonable to suppose that as the wake grows, these large-wavelength fluctuations can become significant, possibly ending or changing the self-similar evolution. If this is true, then any similarity state in a wake could be 'temporary', like the similarity observed in the simulations.

The forcing also has an impact on the vortical structures in the flow, with the forced flow exhibiting large-scale Kármán-vortex-street-like structures similar to those observed in transitional wakes. No such organized structures were present in the unforced flow, where the vorticity was concentrated in a more or less uniform undulating slab without free-stream fluid penetrating deep into the layer. The organized large-scale structure of the strongly forced flow results in strain-dominated 'braid' regions between large-scale structures. Early in the flow evolution it is possible to find streamwise 'rib' vortices within the braid regions, although they do not appear to be as persistent as similar structures in forced mixing layers.

The forcing used in these computations has clearly resulted in qualitative differences in the turbulence. It impacts both the statistics and flow structure and these differences can be maintained for significant time periods, possibly indefinitely. The implications of these observations for the modelling of turbulent wakes are profound. In geometrically equivalent flow situations, it is apparently possible to get wakes with greatly differing growth rates and statistical and structural properties depending on uncontrolled and possibly unknown properties of the initial or inlet conditions. Worse, given the nature of the differences in the initial conditions in the flows studied here, it is likely that standard turbulence models (e.g. k–ϵ or Reynolds stress transport models), which are insensitive to the features of the initial or inlet conditions that control the state of the wake, would be incapable of predicting this flow. This non-uniqueness is important even if it is temporary, since in many situations, the importance of the wake diminishes far from the wake generator.

We thank Professor W. K. George for his help in developing the self-similar analysis presented above for the temporally evolving plane wake and for his insightful comments regarding the evolution of the simulated wake flows. Much of the computations were performed on the NAS supercomputers at the NASA Ames Research Center.

Appendix A. Reynolds stress balances

The governing equation for the evolution of the Reynolds stresses in a time-developing plane wake can be written as

$$\frac{\partial \overline{u_i u_j}}{\partial t} = -\left(\overline{u_i u_l}\frac{\partial \overline{U_j}}{\partial x_l} + \overline{u_j u_l}\frac{\partial \overline{U_i}}{\partial x_l}\right) - \frac{\partial \overline{u_i u_j u_2}}{\partial x_2} - \left(\overline{u_j \frac{\partial (p/\rho)}{\partial x_i}} + \overline{u_i \frac{\partial (p/\rho)}{\partial x_j}}\right) + \nu \frac{\partial^2 \overline{u_i u_j}}{\partial^2 x_2} - 2\nu \overline{\frac{\partial u_i}{\partial x_l}\frac{\partial u_j}{\partial x_l}}. \quad \text{(A 1)}$$

The 'time derivative' on the left is thus composed of 'production', 'turbulent diffusion', 'velocity–pressure gradient', 'viscous diffusion', and 'dissipation' terms, where these terms are given in this order in the above equation (and include minus signs where present). It is also possible to further split the velocity–pressure gradient term into 'pressure–strain' and 'pressure diffusion' terms,

$$-\left(\overline{u_j \frac{\partial (p/\rho)}{\partial x_i}} + \overline{u_i \frac{\partial (p/\rho)}{\partial x_j}}\right) = \overline{\frac{p}{\rho}\left(\frac{\partial u_i}{\partial x_j} + \frac{\partial u_j}{\partial x_i}\right)} - \frac{1}{\rho}\left(\delta_{i2}\frac{\partial \overline{pu_j}}{\partial x_2} + \delta_{j2}\frac{\partial \overline{pu_i}}{\partial x_2}\right). \quad \text{(A 2)}$$

In these equations, only the mean velocity component U_1 is non-zero and due to homogeneity, derivatives of averaged quantities with respect to x_1 and x_3 are zero. Thus, there is no production term in the $\overline{u_2^2}$ and $\overline{u_3^2}$ equations and no pressure diffusion term in the $\overline{u_1^2}$ and $\overline{u_3^2}$ equations. The equation for $q^2 = \overline{u_i u_i}$ can be obtained by contracting the indices in the above equations. For this equation, the pressure–strain is zero and the velocity–pressure gradient term includes only pressure diffusion.

The profiles of each of the terms in the Reynolds stress balance equations (scaled by U_0^3/b with no factors β), time averaged over the self-similar period, are shown in figure 15 for the unforced and weakly forced wake simulations (note that the q^2 balances were shown in figure 12).† The viscous diffusion terms are not plotted because they are an order of magnitude smaller than any other term across the entire layer and thus cannot be distinguished from zero in the figure.‡

If the wakes considered here were exactly self-similar, then the centreline level of $\overline{u_i u_j}/U_0^2$ would remain unchanged. However, since U_0 decays in time, this does not imply that the scaled time derivative (dashed) curves in figure 15 should be zero at $\eta = y/b = 0$. It is possible to use the $\overline{u_i u_j}$ profiles shown in figure 5 with the assumption of self-similarity to derive the entire $\partial \overline{u_i u_j}/\partial t$ profiles, which can then be compared to those in figure 15 to obtain a measure of the departure of the simulations from self-similarity. Generalizing equation (3.30) by defining the functions f_{ij} and g_{ij},

$$f_{ij}(\eta) = \frac{\overline{u_i u_j}(\eta)}{U_0^2}, \quad g_{ij}(\eta) = \frac{b}{U_0^3}\frac{\partial \overline{u_i u_j}(\eta)}{\partial t}, \quad \text{(A 3)}$$

one obtains

$$g_{ij} = -\beta(2f_{ij} + \eta f'_{ij}). \quad \text{(A 4)}$$

At the centreline $g_{ij}(0) = -2\beta f_{ij}(0)$. Obtaining $f_{ij}(0)$ from figure 5 and β from §3.2

† Those for the strongly forced wake flow show significant differences, including overall higher levels (no factors β in the scaling) and turbulent and pressure diffusion dominating production and dissipation. They are not presented here because of the poorer self-similarity of the strongly forced flow.

‡ Note that this is not the case early in the flow evolution, when the initial boundary layer turbulence has significant viscous diffusion near the 'wall', which has just been 'removed'.

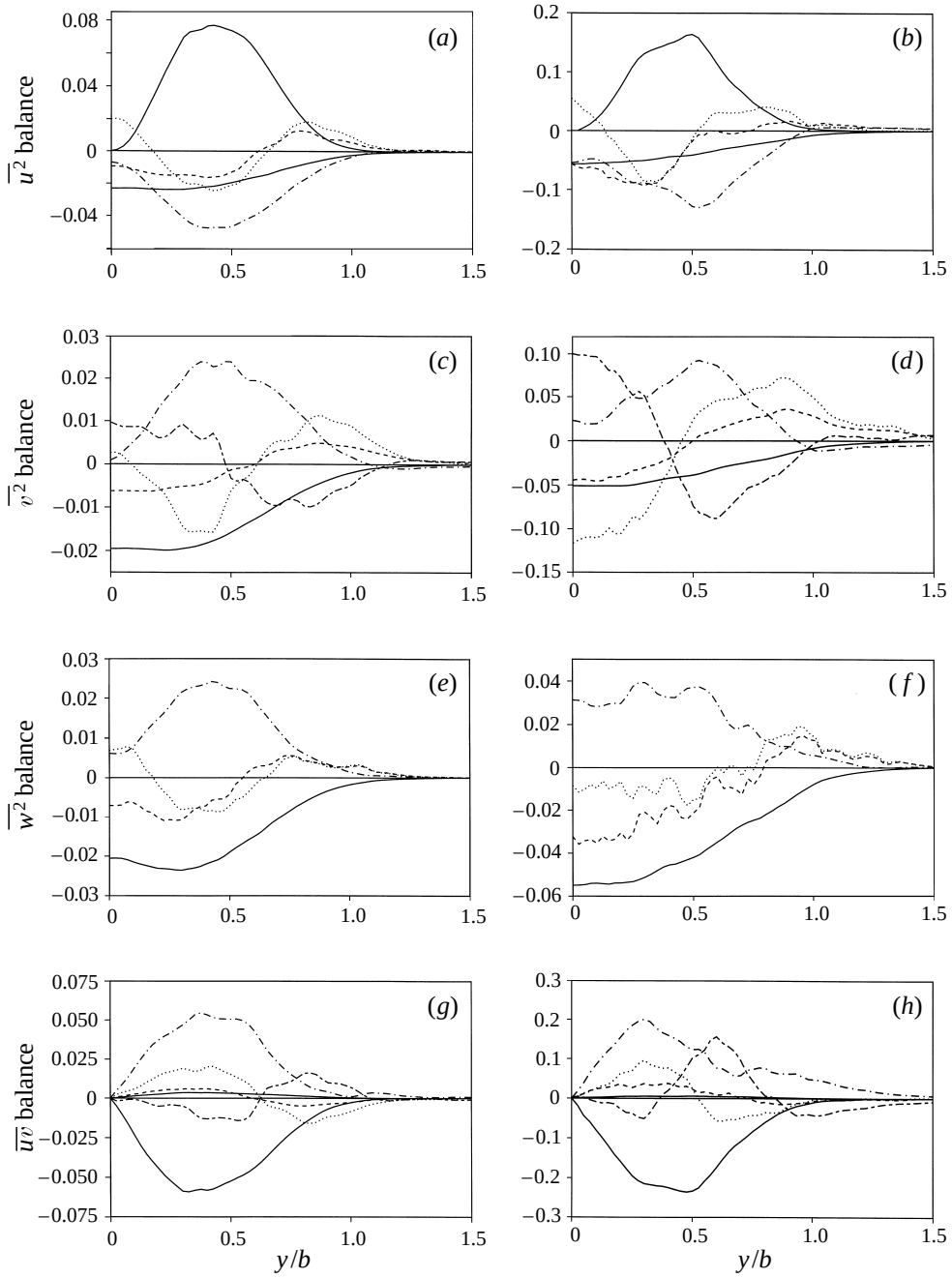

FIGURE 15. Reynolds stress balances for the (*a, b*) $\overline{u^2}$, (*c, d*) $\overline{v^2}$, (*e, f*) $\overline{w^2}$, and (*g, h*) $\overline{uv}$ equations for the unforced (*a, c, e, g*) and weakly forced (*b, d, f, h*) wakes: ———, either production (positive curves in (*a*) and (*b*), negative in (*g*) and (*h*) or dissipation (positive in (*g*) and (*h*), negative in all others); – – – –, time derivative; ·····, turbulent diffusion; —·—, pressure–strain correlation; and — – —, pressure diffusion.

the computed values of $g_{ij}(0)$ can be seen to be in fairly good agreement with the values plotted in figure 15.

Appendix B. Similarity for a passive scalar field

A similarity analysis of the type presented in §3.1 can also be applied to the equations governing the evolution of a passive scalar quantity in the temporally evolving wake flow. In this Appendix two different geometries for the passive scalar field are examined. First, the similarity analysis is applied to a two-stream passive scalar field in which the mean value of the passive scalar differs on the two sides of the wake. Physically, this corresponds to the wake behind a splitter plate separating two equal velocity streams, which each have a different level of the scalar. Next the similarity analysis is extended to a second geometry in which the mean value of the passive scalar on both sides of the wake is equal, but a surplus or deficit of the scalar occurs in the wake. Physically this geometry corresponds to a wake produced behind a hot/cold plane body or the wake produced by a plane body injecting a scalar into the field.

The equation governing the evolution of the mean value of the passive scalar in the temporally evolving wake is given by

$$\frac{\partial \Theta}{\partial t} = -\frac{\partial \overline{v\theta}}{\partial y} + \alpha \frac{\partial^2 \Theta}{\partial y^2} \tag{B 1}$$

where Θ is the mean value of the passive scalar, θ is the scalar fluctuation, and α is the molecular diffusivity of the passive scalar. As in §3.1, it is hypothesized that the equation governing the mean scalar field in the two-stream geometry has a similarity solution of the form

$$\Theta - \Theta_1 = Sc(t)sc(\eta_\theta) \tag{B 2a}$$

$$\overline{v\theta} = R_{v\theta}(t) r_{v\theta}(\eta_\theta), \tag{B 2b}$$

where η_θ is a similarity coordinate based on a characteristic length scale for the passive scalar given by

$$\eta_\theta = \frac{y}{\delta_\theta} \tag{B 3}$$

and Θ_1 is the mean value of the passive scalar in the flow as $y \to -\infty$.

The hypothesized similarity solution given in equation (B 2) must satisfy the boundary conditions as $y \to \pm\infty$. Consequently, the scale for the mean value of the scalar variable must be proportional to the difference of the mean value of the scalar at the two limits; i.e.

$$Sc(t) \propto U_d \Theta = \Theta_2 - \Theta_1, \tag{B 4}$$

where Θ_2 is the mean value of the scalar as $y \to \infty$. It is conventional to define this condition as an equality so $sc(\eta_\theta)$ is a function which varies between 0 and 1.

Substituting the hypothesized similarity solutions into equation (B 1) one obtains

$$-\left[\frac{Sc}{\delta_\theta}\frac{\mathrm{d}\delta_\theta}{\mathrm{d}t}\right]\eta_\theta \frac{\mathrm{d}sc}{\mathrm{d}\eta_\theta} = -\left[\frac{R_{v\theta}}{\delta_\theta}\right]\frac{\mathrm{d}r_{v\theta}}{\mathrm{d}\eta_\theta} + \alpha\left[\frac{Sc}{\delta_\theta^2}\right]\frac{\mathrm{d}^2 sc}{\mathrm{d}\eta_\theta^2}. \tag{B 5}$$

The molecular diffusion terms in this equation are often neglected relative to the turbulent diffusion, but this is not necessary for a similarity solution to exist for this turbulent flow. Consequently, the diffusion terms are not neglected in this analysis.

The hypothesized similarity solutions are consistent with equation (B 1) if

$$\left[\frac{Sc}{\delta_\theta}\frac{\mathrm{d}\delta_\theta}{\mathrm{d}t}\right] \propto \left[\frac{R_{v\theta}}{\delta_\theta}\right] \propto \left[\frac{Sc}{\delta_\theta^2}\right], \tag{B 6}$$

so that

$$R_{v\theta} \propto Sc\frac{\mathrm{d}\delta_\theta}{\mathrm{d}t} \propto U_d\Theta\frac{\mathrm{d}\delta_\theta}{\mathrm{d}t} \tag{B 7}$$

and

$$\frac{\mathrm{d}\delta_\theta^2}{\mathrm{d}t} = \text{constant}. \tag{B 8}$$

Therefore, the proposed similarity solutions are consistent with the equation if the growth rate of the length scale characteristic of the scalar field is given by

$$\delta_\theta \propto (t - t_{o\theta})^{1/2}, \tag{B 9}$$

analogous to the length scale for the velocity field. Note, equation (B 9) does not assume that the virtual origin of the scalar field coincides with the virtual origin of the velocity field. The relationship between the locations of these two virtual origins is deduced below by examining the evolution equation for the passive scalar flux.

As in §3.1, the analysis is next extended to the second-moment equations, here given by evolution equations for the scalar variance and turbulent scalar flux

$$\frac{\partial\overline{\theta^2}}{\partial t} = -2\overline{v\theta}\frac{\partial\Theta}{\partial y} - \frac{\partial\overline{v\theta^2}}{\partial y} + \alpha\frac{\partial^2\overline{\theta^2}}{\partial y^2} - \epsilon_\theta, \tag{B 10a}$$

$$\frac{\partial\overline{u\theta}}{\partial t} = -\overline{\frac{\theta}{\rho}\frac{\partial p}{\partial x}} - \overline{v\theta}\frac{\partial\delta U}{\partial y} - \overline{uv}\frac{\partial\Theta}{\partial y} - \frac{\partial\overline{uv\theta}}{\partial y} + \alpha\frac{\partial}{\partial y}\overline{u\frac{\partial\theta}{\partial y}} + \nu\frac{\partial}{\partial y}\overline{\theta\frac{\partial u}{\partial y}} - \epsilon_{u\theta}, \tag{B 10b}$$

$$\frac{\partial\overline{v\theta}}{\partial t} = -\overline{\frac{\theta}{\rho}\frac{\partial p}{\partial y}} - \overline{v^2}\frac{\partial\Theta}{\partial y} - \frac{\partial\overline{v^2\theta}}{\partial y} + \alpha\frac{\partial}{\partial y}\overline{v\frac{\partial\theta}{\partial y}} + \nu\frac{\partial}{\partial y}\overline{\theta\frac{\partial v}{\partial y}} - \epsilon_{v\theta}, \tag{B 10c}$$

where ϵ_θ, $\epsilon_{u\theta}$, and $\epsilon_{v\theta}$ are dissipation rates given by

$$\epsilon_\theta = 2\alpha\left\{\overline{\left(\frac{\partial\theta}{\partial x}\right)^2} + \overline{\left(\frac{\partial\theta}{\partial y}\right)^2} + \overline{\left(\frac{\partial\theta}{\partial z}\right)^2}\right\}, \tag{B 11a}$$

$$\epsilon_{u\theta} = (\nu + \alpha)\left\{\overline{\frac{\partial u}{\partial x}\frac{\partial\theta}{\partial x}} + \overline{\frac{\partial u}{\partial y}\frac{\partial\theta}{\partial y}} + \overline{\frac{\partial u}{\partial z}\frac{\partial\theta}{\partial z}}\right\}, \tag{B 11b}$$

and

$$\epsilon_{v\theta} = (\nu + \alpha)\left\{\overline{\frac{\partial v}{\partial x}\frac{\partial\theta}{\partial x}} + \overline{\frac{\partial v}{\partial y}\frac{\partial\theta}{\partial y}} + \overline{\frac{\partial v}{\partial z}\frac{\partial\theta}{\partial z}}\right\}. \tag{B 11c}$$

Using the definitions given in table 1 in §3.1 and table 2, a similarity solution is possible when

$$\left[\frac{\mathrm{d}V_\theta}{\mathrm{d}t}\right] \propto \left[\frac{V_\theta}{\delta_\theta}\frac{\mathrm{d}\delta_\theta}{\mathrm{d}t}\right] \propto \left[\frac{Tt_\theta}{\delta_\theta}\right] \propto \left[\frac{V_\theta}{\delta_\theta^2}\right] \propto \left[\frac{R_{v\theta}Sc}{\delta_\theta}\right] \propto [D_\theta], \tag{B 12a}$$

$$\left[\frac{\mathrm{d}R_{u\theta}}{\mathrm{d}t}\right] \propto \left[\frac{R_{u\theta}}{\delta_\theta}\frac{\mathrm{d}\delta_\theta}{\mathrm{d}t}\right] \propto [\Pi_{u\theta}] \propto \left[\frac{R_{v\theta}U_s}{\delta}\right] \propto \left[\frac{R_sSc}{\delta_\theta}\right] \propto \left[\frac{Tt_{u\theta}}{\delta_\theta}\right] \propto \left[\frac{M_{u\theta}}{\delta_\theta}\right] \propto \left[\frac{R_{u\theta}}{\delta_\theta^2}\right] \propto [D_{u\theta}], \tag{B 12b}$$

Term	Form	Similarity conditions
$\Theta - \Theta_1$	$Sc(t)sc(\eta_\theta)$	$Sc \propto U_d\Theta$ or $\dfrac{1}{\delta_\theta}$
$\overline{\theta^2}$	$V_\theta(t)v_\theta(\eta_\theta)$	$V_\theta \propto Sc^2$
$\overline{u\theta}$	$R_{u\theta}(t)r_{u\theta}(\eta_\theta)$	$R_{u\theta} \propto Sc\dfrac{\mathrm{d}\delta_\theta}{\mathrm{d}t}$
$\overline{v\theta}$	$R_{v\theta}(t)r_{v\theta}(\eta_\theta)$	$R_{v\theta} \propto Sc\dfrac{\mathrm{d}\delta_\theta}{\mathrm{d}t}$
$\overline{\dfrac{p}{\rho}\dfrac{\partial\theta}{\partial x}}$	$\Pi_{u\theta}(t)\pi_{u\theta}(\eta_\theta)$	$\Pi_{u\theta} \propto \dfrac{Sc}{\delta_\theta^2}\dfrac{\mathrm{d}\delta_\theta}{\mathrm{d}t}$
$\overline{\dfrac{p}{\rho}\dfrac{\partial\theta}{\partial y}}$	$\Pi_{v\theta}(t)\pi_{v\theta}(\eta_\theta)$	$\Pi_{v\theta} \propto \dfrac{Sc}{\delta_\theta^2}\dfrac{\mathrm{d}\delta_\theta}{\mathrm{d}t}$
$\overline{v\theta^2}$	$Tt_\theta(t)tt_\theta(\eta_\theta)$	$Tt_\theta \propto Sc^2\dfrac{\mathrm{d}\delta_\theta}{\mathrm{d}t}$
$\overline{uv\theta}$	$Tt_{u\theta}(t)tt_{u\theta}(\eta_\theta)$	$Tt_{u\theta} \propto \dfrac{Sc}{\delta_\theta}\dfrac{\mathrm{d}\delta_\theta}{\mathrm{d}t}$
$\overline{v^2\theta}$	$Tt_{v\theta}(t)tt_{v\theta}(\eta_\theta)$	$Tt_{v\theta} \propto \dfrac{Sc}{\delta_\theta}\dfrac{\mathrm{d}\delta_\theta}{\mathrm{d}t}$
$\overline{\dfrac{p\theta}{\rho}}$	$Pt_{v\theta}(t)pt_{v\theta}(\eta_\theta)$	$Pt_{v\theta} \propto \dfrac{Sc}{\delta_\theta}\dfrac{\mathrm{d}\delta_\theta}{\mathrm{d}t}$
$\overline{u\dfrac{\partial\theta}{\partial y}}$	$M_{u\theta}(t)m_{u\theta}(\eta_\theta)$	$M_{u\theta} \propto \dfrac{Sc}{\delta_\theta}\dfrac{\mathrm{d}\delta_\theta}{\mathrm{d}t}$
$\overline{v\dfrac{\partial\theta}{\partial y}}$	$M_{v\theta}(t)m_{v\theta}(\eta_\theta)$	$M_{v\theta} \propto \dfrac{Sc}{\delta_\theta}\dfrac{\mathrm{d}\delta_\theta}{\mathrm{d}t}$
ϵ_θ	$D_\theta(t)d_\theta(\eta_\theta)$	$D_\theta \propto \dfrac{Sc^2}{\delta_\theta}\dfrac{\mathrm{d}\delta_\theta}{\mathrm{d}t}$
$\epsilon_{u\theta}$	$D_{u\theta}(t)d_{u\theta}(\eta_\theta)$	$D_{u\theta} \propto \dfrac{Sc}{\delta_\theta^2}\dfrac{\mathrm{d}\delta_\theta}{\mathrm{d}t}$
$\epsilon_{v\theta}$	$D_{v\theta}(t)d_{v\theta}(\eta_\theta)$	$D_{v\theta} \propto \dfrac{Sc}{\delta_\theta^2}\dfrac{\mathrm{d}\delta_\theta}{\mathrm{d}t}$

TABLE 2. Similarity forms for terms in the scalar equations

$$\left[\frac{\mathrm{d}R_{v\theta}}{\mathrm{d}t}\right] \propto \left[\frac{R_{v\theta}}{\delta_\theta}\frac{\mathrm{d}\delta_\theta}{\mathrm{d}t}\right] \propto [\Pi_{v\theta}] \propto \left[\frac{Pt_{v\theta}}{\delta_\theta}\right] \propto \left[\frac{K_v Sc}{\delta_\theta}\right] \propto \left[\frac{Tt_{v\theta}}{\delta_\theta}\right] \propto \left[\frac{M_{v\theta}}{\delta_\theta}\right] \propto \left[\frac{R_{v\theta}}{\delta_\theta^2}\right] \propto [D_{v\theta}]\,. \tag{B 12c}$$

The first term in equation (B 12*a*) is included to allow for the general possibility that the scale for the scalar variance is a function of time. If this is not the case (as in this first scalar geometry being considered), the term is zero and consequently does not appear in the equation or provide a constraint for the similarity analysis.

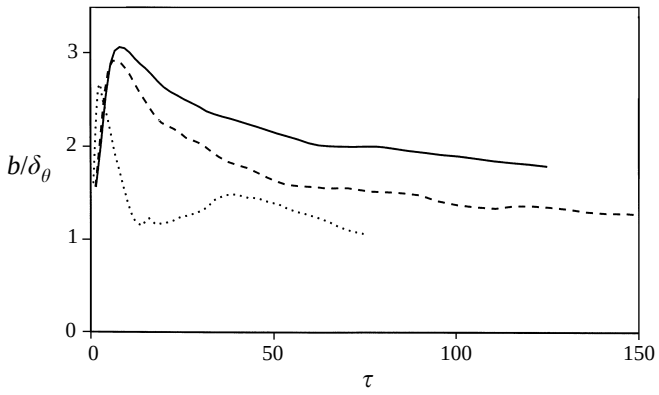

FIGURE 16. Hydrodynamic to scalar width ratio for the ———, unforced; – – – –, weakly forced; and ·····, strongly forced wake simulations.

The proportionality of the second and fifth terms in equation (B 12*a*) implies that

$$V_\theta \propto (Sc)^2 \propto (U_d\Theta)^2. \tag{B 13}$$

Thus, the similarity scale for the scalar variance is independent of time in this two-stream geometry. As noted above, in this case the first constraint in equation (B 12*a*) would not appear because this term is zero in the original equation. The scales for the other moments in the scalar variance equation are given in table 2.

The proportionality of the second and fifth terms in equation (B 12*c*) results in

$$\left(\frac{\mathrm{d}\delta_\theta}{\mathrm{d}t}\right)^2 \propto U_s^2, \tag{B 14}$$

or

$$\frac{1}{\delta_\theta^2} \propto \frac{1}{\delta^2}, \tag{B 15}$$

implying

$$(t - t_{o\theta})^{-1} \propto (t - t_o)^{-1}, \tag{B 16}$$

where t_o is the location of the virtual origin for the velocity field and $t_{o\theta}$ is the virtual origin for the scalar field. This condition can also be written as

$$\frac{t - t_{o\theta}}{t - t_o} = \text{constant}, \tag{B 17}$$

from which it is clear that a similarity solution can only exist for the equations governing the scalar field if the virtual origin of the scalar field is located at the same point as the virtual origin of the velocity field. Note that this condition can also be derived from the proportionality of the fourth and fifth terms in equation (B 12*c*).

Although not needed to close the mean scalar equation, the streamwise scalar flux $\overline{u\theta}$ is also non-zero in this flow as a result of the mean shear. The terms in this equation provide no additional constraints on the self-similar solution; their form is also given in table 2.

In all three wake flows, the evolution of a passive scalar field of the type discussed above (ranging from zero to one in the two free streams) has been calculated along with the hydrodynamic flow field. Although the terms in the equations governing the second-order moments of the scalar statistics have not been examined, the behaviour of the mean scalar field, the scalar fluctuation intensity, and both components of the

scalar flux have been studied for the unforced case. All of these quantities appear to be evolving self-similarly over the self-similar period of the hydrodynamic evolution as evidenced by reasonable collapse of the profiles when scaled by the appropriate variables. Although the length scale b does a fair job of collapsing profiles from different times, better collapse is obtained by scaling with a scalar thickness δ_θ derived from the mean scalar profile. Here δ_θ is taken to be the distance between the points where $\Theta = 0.25$ and $\Theta = 0.75$. Figure 16 contains the time evolution of the ratio b/δ_θ. For all cases this ratio is approximately constant over the self-similar periods defined previously, as required for self-similarity from equation (B 15). Note that the ratio between δ_θ of an error function and b of its derivative (a Gaussian) is given by $b/\delta_\theta = 1.75$, which lies between the unforced and weakly forced cases in figure 16.

The analysis of the scalar field in a temporally evolving plane wake flow can easily be extended to a second geometry in which there is a scalar deficit or surplus in the wake. The analysis for all of the higher-order moments is the same as the analysis for the previous geometry. The only difference between the two problems is that the scale for the mean value of the scalar differs. Thus, all that is necessary to extend the analysis to this second geometry is an analysis of the equation for the mean value of the scalar. When a scalar deficit occurs in the wake it is conventional to write the equation in a deficit form; i.e.

$$\frac{\partial(\Theta_\infty - \Theta)}{\partial t} = \frac{\partial \overline{v\theta}}{\partial y} + \alpha \frac{\partial^2(\Theta_\infty - \Theta)}{\partial y^2} \tag{B 18}$$

where Θ_∞ is the value of the scalar in the free stream. This equation can be integrated to yield

$$\frac{\partial}{\partial t} \int_{-\infty}^{\infty} (\Theta_\infty - \Theta)\, \mathrm{d}y = 0 \tag{B 19}$$

if it is assumed that there is no free-stream turbulence and the effect of the diffusion goes to zero as $y \to \pm\infty$.

Thus, if it is hypothesized that similarity solutions of the form

$$\Theta_\infty - \Theta = Sc(t) sc(\eta_\theta) \tag{B 20}$$

and

$$\overline{v\theta} = R_{v\theta}(t) r_{v\theta}(\eta_\theta) \tag{B 21}$$

exist for the present geometry, it follows that these solutions are consistent with the equations for the mean scalar if

$$Sc\delta_\theta \propto \text{constant} \tag{B 22a}$$

$$\left[\frac{\mathrm{d}Sc}{\mathrm{d}t}\right] \propto \left[\frac{Sc}{\delta_\theta}\frac{\mathrm{d}\delta_\theta}{\mathrm{d}t}\right] \propto \left[\frac{R_{v\theta}}{\delta_\theta}\right] \propto \left[\frac{Sc}{\delta_\theta^2}\right]. \tag{B 22b}$$

Thus, for the deficit flow

$$Sc \propto \frac{1}{\delta_\theta}, \tag{B 23a}$$

$$\frac{\mathrm{d}\delta_\theta^2}{\mathrm{d}t} \propto \text{constant}, \tag{B 23b}$$

which is analogous to the conditions derived for the velocity field. The scale for all of the higher-order moments can also be deduced from the analysis of the equations outlined above, but using the new scale Sc for the mean scalar field.

REFERENCES

Antonia, R. A., Browne, L. W. B. & Bisset, D. K. 1987 A description of the organized motion in the turbulent far wake of a cylinder at low reynolds number. *J. Fluid Mech.* **184**, 423–444.

Browand, F. K. & Troutt, T. R. 1980 A note on spanwise structure in the two-dimensional mixing layer. *J. Fluid Mech.* **97**, 771–781.

Ewing, D. 1995 On Multi-Point Similarity Solutions in Turbulent Free-Shear Flows. PhD thesis, State University of New York at Buffalo.

Ewing, D. W., Rogers, M. R., George, W. K. & Moser, R. D. 1998 On the similarity of the two-point correlation tensor in a turbulent temporally evolving plane wake. In preparation.

George, W. K. 1989 The self-preservation of turbulent flows and its relation to initial conditions and coherent structure. In *Advances in Turbulence* (ed. W. K. George & R. Arndt), pp. 39–73. Hemisphere.

George, W. K. 1994 Some new ideas for similarity of turbulent shear flows. In *Proc. Intl Symp. on Turbulent Heat and Mass Transfer, Lisbon Portugal.*

Ghosal, S. & Rogers, M. M. 1997 A numerical study of self-similarity in a turbulent plane wake using large eddy simulation. *Phys. Fluids* **9**, 1729–1739.

Hayakawa, M. & Hussain, F. 1989 Three-dimensionality of organized structures in a plane wake. *J. Fluid Mech.* **206**, 375–404.

Lasheras, J. C. & Meiburg, E. 1990 Three-dimensional vorticity modes in the wake of a flat plate. *Phys. Fluids* A **2**, 371–380.

Marasli, B., Champagne, F. H. & Wygnanski, I. 1992 Effect of traveling waves on the growth of a plane turbulent wake. *J. Fluid Mech.* **235**, 511–528.

McIlwain, S., Ewing, D. & Pollard, A. 1997 Evolution of large- and small-scale coherent structures in non-homogeneous shear flows. *Bull. Am. Phys. Soc.* **41**, 1816.

Narasimha, R. 1989 The utility and drawbacks of traditional approaches. In *Whither Turbulence* (ed. J. Lumley). Springer.

Oberlack, M. 1997 Unified theory for symmetries in plane turbulent shear flows. *J. Fluid Mech.* (submitted).

Prabhu, A. & Narasimha, R. 1972 Turbulent non-equilibrium wakes. *J. Fluid Mech.* **54**, 19–38.

Rogers, M. M. & Moin, P. 1987 The structure of the vorticity field in homogeneous turbulent flows. *J. Fluid Mech.* **176**, 33–66.

Rogers, M. M. & Moser, R. D. 1993 The three-dimensional evolution of a plane mixing layer: the kelvin-helmholtz rollup. *J. Fluid. Mech.* **243**, 183–226.

Rogers, M. M. & Moser, R. D. 1994 Direct simulation of a self-similar turbulent mixing layer. *Phys. Fluids* **6**, 903–923.

Spalart, P. R. 1988 Direct simulation of a turbulent boundary layer up to $Re_\theta = 1410$. *J. Fluid Mech.* **187**, 61–98.

Spalart, P. R., Moser, R. D. & Rogers, M. M. 1991 Spectral methods for the navier–stokes equations with one infinite and two periodic directions. *J. Comput. Phys.* **96**, 297–324.

Sreenivasan, K. R. & Narasimha, R. 1982 Equilibrium parameters for two-dimensional turbulent wakes. *Trans. ASME* I: *J. Fluids Engng* **104**, 167–170.

Tennekes, H. & Lumley, J. L. 1972 *A First Course in Turbulence*. MIT Press.

Townsend, A. A. 1976 *Structure of Turbulent Shear Flow*. Cambridge University Press.

Weygandt, J. H. & Mehta, R. D. 1995 Three-dimensional structure of straight and curved plane wakes. *J. Fluid Mech.* **282**, 279–311.

Wygnanski, I., Champagne, F. & Marasli, B. 1986 On the large-scale structures in two-dimensional small-deficit, turbulent wakes. *J. Fluid Mech.* **168**, 31–71.